GeoExpert ag

swiss*nuclear*: PEGASOS Refinement Project:
SP2 – Ground Motion Characterization

Contract no. PMT-VT-1032

Seismic Shear Wave Velocity Determination and Hybrid Seismic Survey at the SED-Station GIMEL (St. Georges, VD)

Date of Field Data Acquisition 18th May 2009

Report

Client

swiss*nuclear*
Project PRP
Frohburgstrasse 17
4601 Olten

Contractor

GeoExpert ag
Seismic Prospecting
Ifangstrasse 12b
P.O. Box 451
8603 Schwerzenbach

8603 Schwerzenbach, 1st July 2009

INDEX

1 INTRODUCTION....3
1.1 Survey objectives....3
1.2 The choice of the appropriate surveying methods....3
2 FIELD DATA ACQUISITION PARTICULARS....4
2.1 Time Schedule....4
2.2 Summary of Data Acquisition Parameters....4
2.3 Composition of Seismic Field Crew....5
2.4 Location....5
2.5 Recording Conditions and Line Setup....5
3 SEISMIC DATA PROCESSING AND IMAGING OF THE RESULTS....7
3.1 General Remarks....7
3.2 Shear Wave Refraction Tomography....7
3.2.1 Reformatting and field geometry assignment....7
3.2.2 First break time picking....7
3.2.3 Analytical Determination of Refraction Velocities....8
3.2.4 Tomographic inversion of the velocity gradient field by iterative modeling....9
3.3 MASW Processing....12
3.3.1 Reformatting and field geometry assignment....12
3.3.2 Calculating the dispersion image (overtone)....12
3.3.3 Analysis of the dispersion image....12
3.3.4 Inversion of dispersion curves resulting in a 1D shear wave velocity distribution....15
3.3.5 Gridding and plotting of 2D v_s-velocity field....18
3.3.6 Calculation of the average shear wave velocity....19
3.3.7 Calculation of the shear wave velocity scalars $v_{s,5}$, $v_{s,10}$, ...21
3.4 Hybrid Seismic Data Processing....22
3.4.1 p-wave Reflection Seismic Processing Sequence....22
3.4.2 The presentation of reflection seismic data....22
3.4.3 p-wave refraction tomography processing....25
3.4.4 Representation of the hybrid seismic section....30
4 DISCUSSION OF THE RESULTS 31
4.1 Summary and Validation of the Results....31
4.2 Validation of the methods and their results....32
4.3 Error Estimates....32
4.4 The Geophysical Interpretation....33
5 SUMMARY AND CONCLUSIONS....35

1 INTRODUCTION

1.1 Survey objectives

The seismic survey's main task is to provide information about the distribution function of the shear wave velocities in the depth interval of the uppermost 30 m along a 100 m long seismic profile.

Additionally, the following objectives are to be met:

- the mapping of the topography of the rock face, i.e. the thickness of the Quaternary deposits;
- the determination of the thickness of the weathered zone and its degree of decompaction at the bedrock surface;
- a general view of geological structures.

1.2 The choice of the appropriate surveying methods

Several methods are available for deriving the s-wave velocity distribution in the subsurface at any given position:

- in-situ measurement by down-hole or crosshole seismic surveying;
- shear-wave refraction tomography profiling;
- dispersion analysis of surface waves (MASW; **M**ultiple channel **A**nalysis of **S**urface **W**aves)

The surveys are to be carried out at, or as close as possible near some 20 SED earth quake monitoring stations in Switzerland. Ideally, the surveys are to be conducted on two orthogonal profiles in order to derive at their point of intersection a robust 1D s-wave velocity distribution function by correlation. To this end, the methods of MASW and shear-wave refraction tomography profiling are to be combined.

The results are to include the following fundamental parameters $v_{s,5}$, $v_{s,10}$, $v_{s,20}$, $v_{s,30}$, $v_{s,40}$, $v_{s,50}$, $v_{s,100}$ are to be calculated, also an error estimation of all values.

The data acquired for the MASW method are to be subjected to complementary **p-wave hybrid seismic data processing** in order to image the geological structures.

2 FIELD DATA ACQUISITION PARTICULARS

2.1 Time Schedule

Date	*Time*	*Activities / remarks*
18.05.2009	1000	arrival at site
	1000 - 1115	site investigation (included: searching the SED-Station)
	1115 - 1215	lay-out of spread profile 1 (p-wave and s-wave)
	1255 - 1330	data acquisition of spread profile 1 (p-wave)
	1350 - 1435	data acquisition of spread profile 1 (s-wave)
	1435 - 1540	lay-out of spread profile 2 (p-wave and s-wave)
	1540 - 1605	data acquisition of spread profile 2 (p-wave)
	1625 - 1710	data acquisition of spread profile 2 (s-wave)
	1710 - 1745	removal of the seismic measuring system
	1745	departure from site

2.2 Summary of Data Acquisition Parameters

Compressional Wave Data Acquisition

# of active channels	96
geophone type	4.5 Hz natural frequency, vertical velocimeter
receiver station spacing	1.0 m
# of geophones/station	1
source point spacing	2.0 m to 3.0 m
source type	vertical hammer (8 kg) striking on a horizontal metal plate
sampling rate	500 µs
recording time	2048 ms
field filters	0.5 Hz LC, anti-alias
# of field records	48 (line 09SN_08GIMEL-P1) and 50 (line 09SN_08GIMEL-P2)

Shear Wave Data Acquisition

# of active channels	48
geophone type	10 Hz natural frequency, horizontal velocimeter
receiver station spacing	2.0 m
# of geophones/station	1
source point spacing	4.0 m to 6.0 m
source type	horizontal hammer (8 kg) striking horizontally at a metal-plated wooden beam anchored to the ground by means of 20 cm long spikes
sampling rate	500 µs
recording time	512 ms
field filters	2 Hz LC, anti-alias
# of field records	50 (line 09SN_08GIMEL-S1) and 51 (line 09SN_08GIMEL-S2)

Fig. 2.1: Data acquisition at profile 09SN_08GIMEL-1.

2.3 Composition of Seismic Field Crew

Personnel

Jochen Fiseli	Dipl.-Geologist, University of Freiburg i. Br., party chief
Fabian Isler	assistant, spread lay-out and activation of seismic source
Michael Kuhlmann	assistant, spread lay-out and activation of seismic source

Equipment

96	vertical geophones 4.5 Hz
48	horizontal geophones 12 Hz
6	seismic cables
1	seismic acquisition system Summit Compact, 96 channels
1	laptop computer for data acquisition
3	walkie-talkies
1	hammer 6 kg
1	steel plate
1	metal-plated wooden beam
1	van (FIAT Ducato 4x4)

2.4 Location

The seismic monitoring station GIMEL (St. Georges, VD) is situated in a military cavern in a Lower Cretaceous sediment unit covering the widespread Malm rock plateau in the Jura range, Western Switzerland, canton of Vaud. The measurements are accomplished on the Cretaceous cliff, some handful of meters above the seismic station. Partly, the soil thickness may span over a few meters.

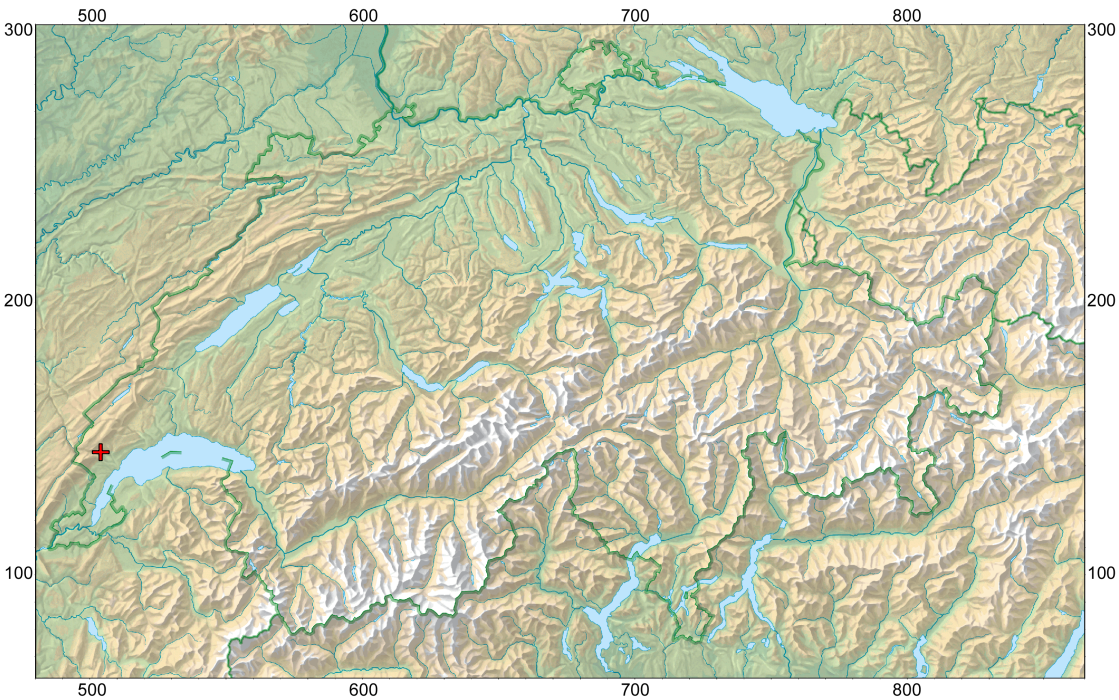

Fig. 2.2: The red cross marked seismic monitoring station GIMEL (St. Georges, NE) is located in Lower Cretaceous sediments. (map: geodata @ swisstopo).

2.5 Recording Conditions and Line Setup

Sunny weather and moderate temperatures prevailed throughout the field data recording period. In general, the data quality obtained at GIMEL is to be rated as good.

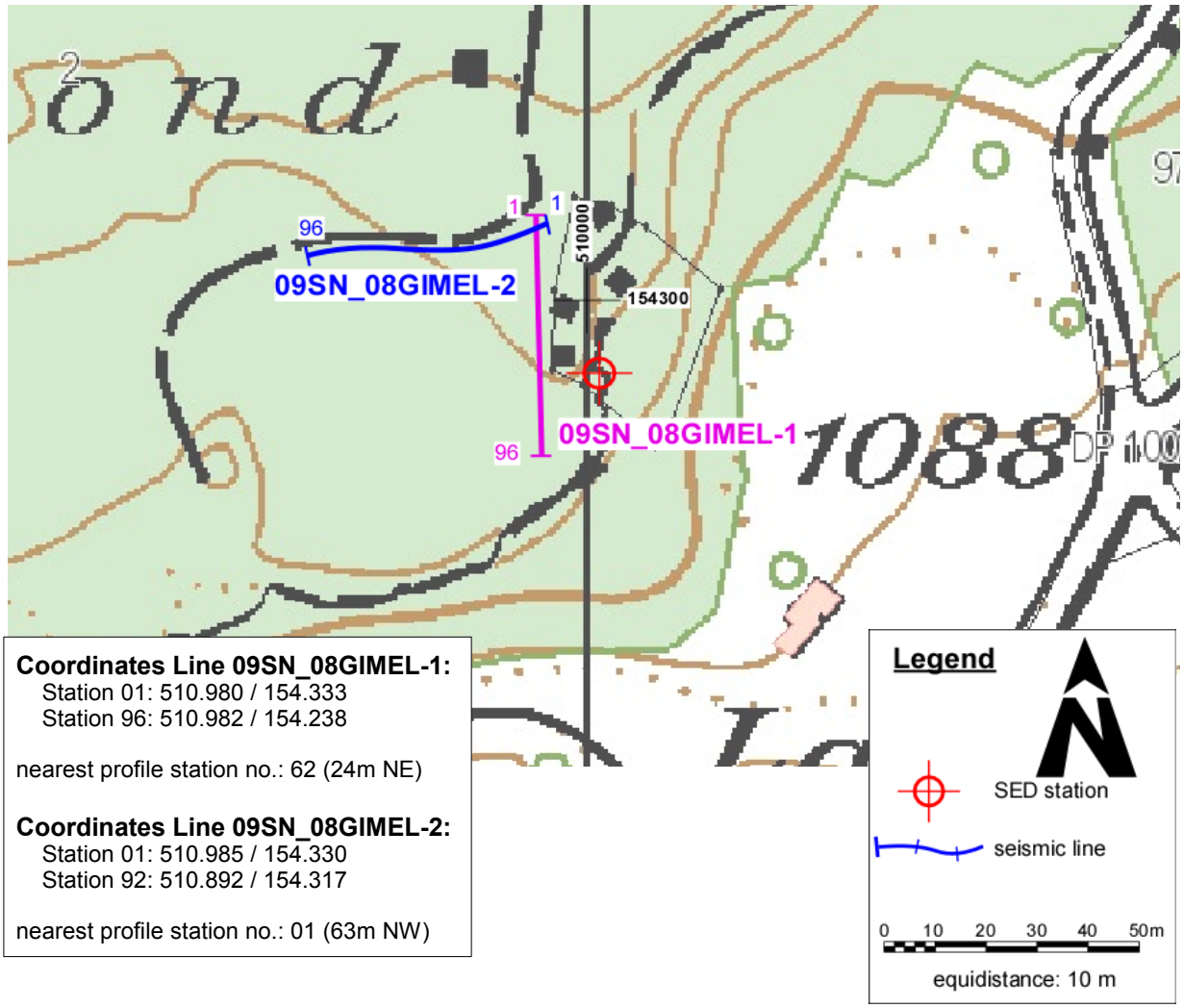

Fig. 2.3: Situation map with the trace of seismic profile 09SN_08GIMEL-1 and -2. (© Etat de Vaud, swisstopo, cartosphere - informations dépourvues de foi publique).

3 SEISMIC DATA PROCESSING AND IMAGING OF THE RESULTS

3.1 General Remarks

- For the shear and compressional wave refraction seismic evaluation the package **RAYFRACT** by Intelligent Resources Ltd., Vancouver CAN, was used. The system features the technique of diving wave tomography (www.rayfract.com).
- The system **SPW** (**S**eismic **P**rocessing **W**orkshop) of Parallel Geoscience Corporation, Austin US-TX, was used for reflection seismic data processing (www.parallelgeo.com).
- Data processing of surface waves (MASW processing) was conducted with the software package **SurfSeis** V2.0 of Kansas Geological Survey in Lawrence US-KS.

A detailed description of the various surveying methods will be included in the general summary report.

3.2 Shear Wave Refraction Tomography

3.2.1 Reformatting and field geometry assignment

After reformatting the field data into the Rayfract format the field geometry is applied.

3.2.2 First break time picking

At each shot position, two seismic records were acquired in both activation directions. These two records are displayed superimposed with different colors on each other in Fig 3.2a together with the manually determined first arrival time picks.

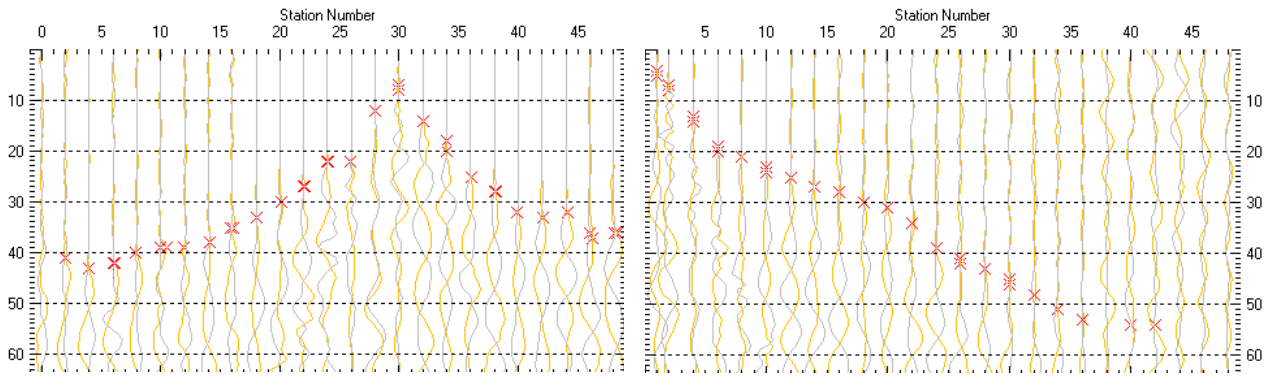

*Fig. 3.2a: High quality dual field record of line 09SN_08GIMEL-S1 (left) and -S2 (right).showing at each station the s-wave traces with opposing polarities in different colors. The manually picked s-wave refraction arrivals at each station are marked with an **x**. The station spacing is 2 m, profile station number 00 = profile meter 0; profile station number 48 = profile meter 96.*

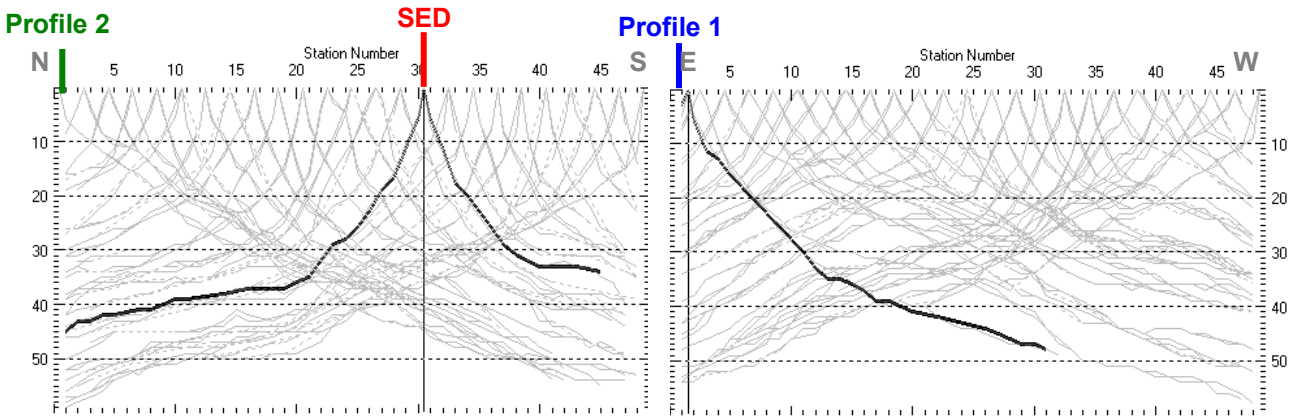

Fig. 3.2b: Curves of s-wave first break time picks of line 09SN_08GIMEL-S1 (left) and -S2 (right).

3.2.3 Analytical Determination of Refraction Velocities

An initial 1D-velocity function (averaged 1D velocity-depth profiles derived by the Delta-t-V method, see Tab. 3.2a) is determined in the 3-dimensional time-offset-CMP-domain of all first break arrival time curves in the 3-dimensional time-offset-CMP-domain (see. Fig. 3.2c).

Depth [m]	Vs [m/s]
0.0	282
0.4	347
0.7	424
1.1	477
1.6	570
2.1	666
3.0	829
4.1	1021
5.7	1334
7.5	1621
10.1	2120
13.3	2664
17.6	3304
23.3	4063
30.6	4617
40.4	4265

Depth [m]	Vs [m/s]
0.0	423
0.4	506
0.7	597
1.1	673
1.6	783
2.1	887
3.0	1062
4.0	1275
5.6	1487
7.4	1646
10.0	1866
13.2	2202
17.4	2779
23.0	3245
30.2	3515
39.8	4372

Tab. 3.2a: Initial 1D s-wave velocity function derived from real data of line 09SN_08GIMEL-S1 (mean values of all computed models) and of line -S2 (mean values of all computed models).

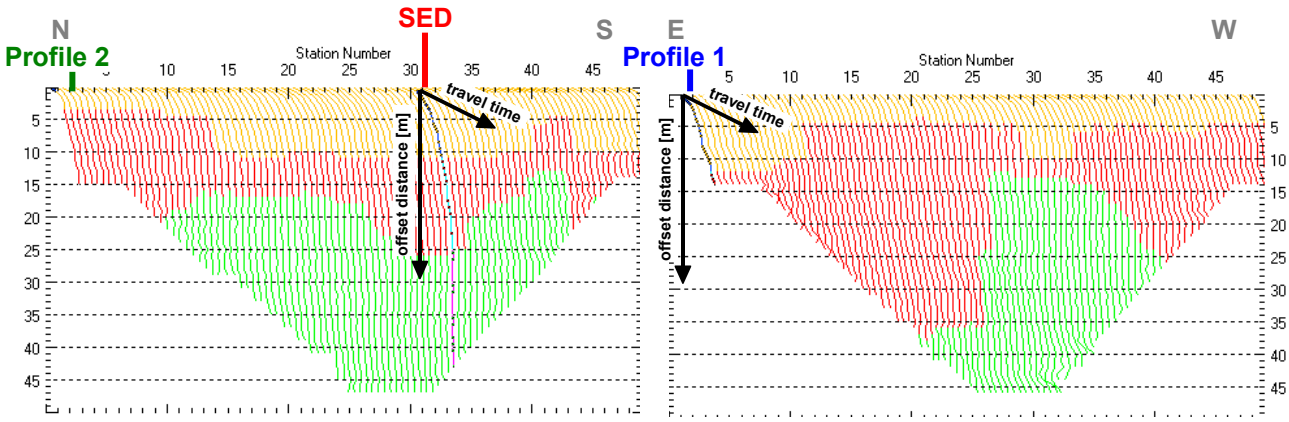

Fig. 3.2c: 3-dimensional distance-travel time diagrams of line 09SN_08GIMEL-S1 (left) and -S2 (right) at the mid-points between source points and receiver stations are instrumental when using the analytical CMP derivation of the initial velocity field.
The horizontal axes are the along the CMP positions and the travel time respectively, the vertical axis denotes the offset distance between source and receiver positions. The colors represent different velocity layers. The station spacing is 2 m, profile station number 00 = profile meter 0; profile station number 48 = profile meter 96. The colors represent different velocity layers.

3.2.4 Tomographic inversion of the velocity gradient field by iterative modeling

The velocity field is iteratively refined by the subsequent Wavepath Eikonal Traveltime (WET) tomographic inversion process. The inversion results are portrayed in Fig. 3.2d as a gridded velocity contour section and in Fig. 3.2e as a ray path density section.

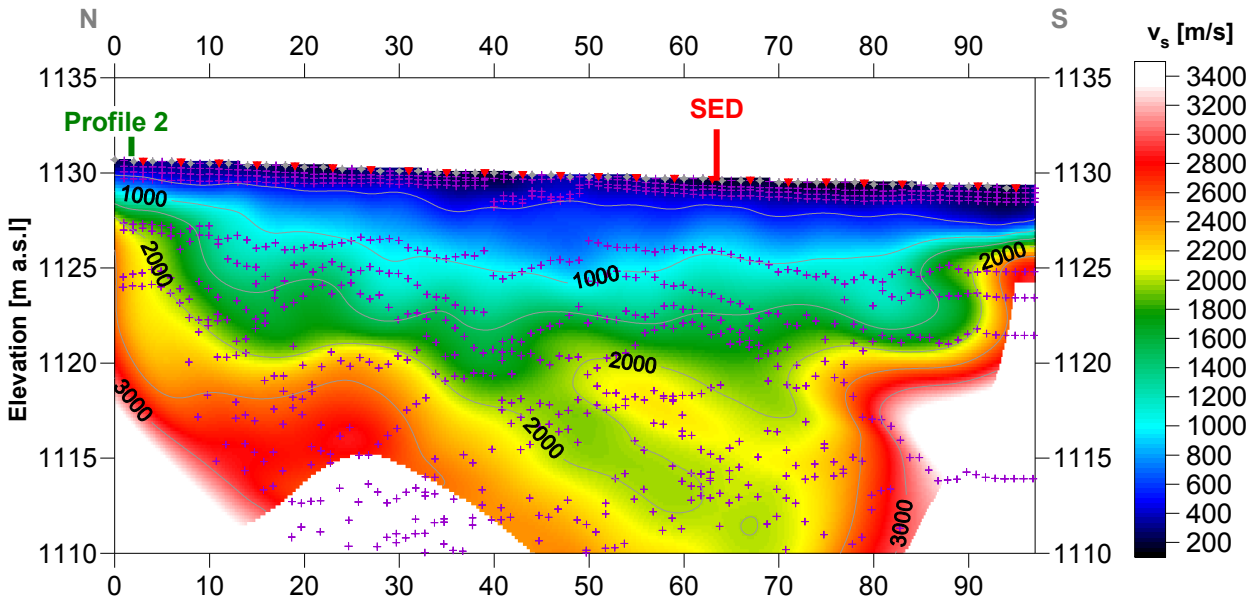

Fig. 3.2d: Shear wave velocity field of the line 09SN_08GIMEL-S1. Red/white colors denote solid rock, blue/black colors point to unconsolidated sediments and soil.
Vertical axis: elevation [m a.s.l]; horizontal axis: profile meter; color encoded scale: v_s [m/s]; vertical exaggeration: 2:1; gray diamonds: receiver positions; red triangles: source positions; magenta crosses: positions of determined velocity values. The station spacing is 2 m, profile meter 0 = profile station number 00, profile meter 96 = profile station number 48.

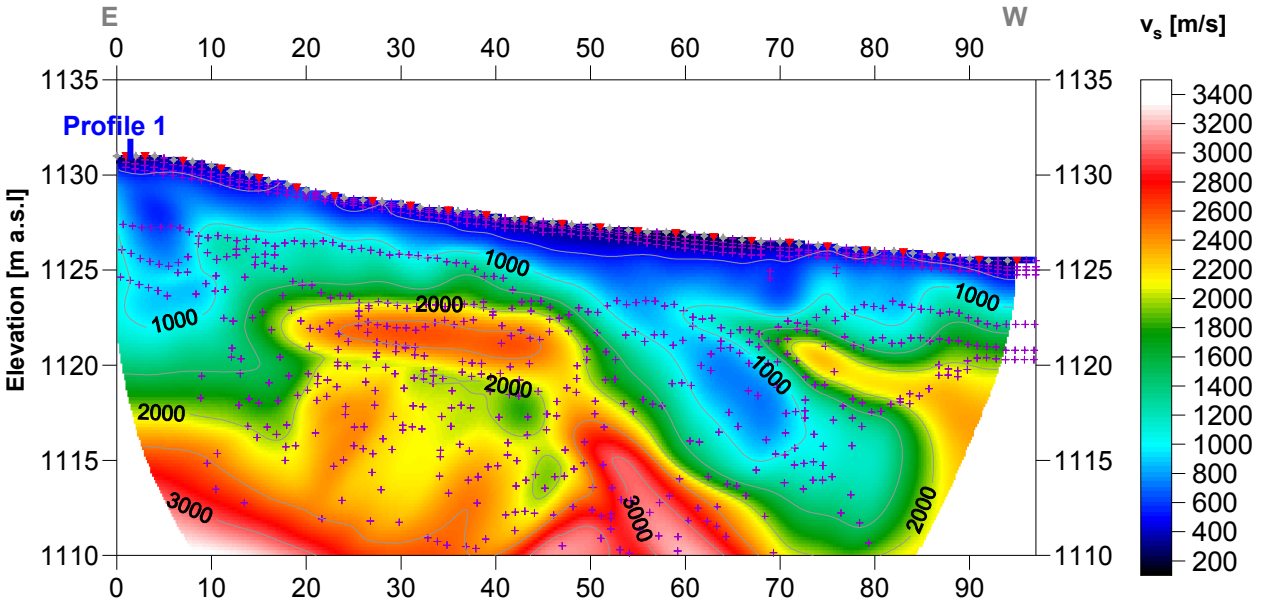

Fig. 3.2e: Shear wave velocity field of the line 09SN_08GIMEL-S2. Red/white colors denote solid rock, blue/black colors point to unconsolidated sediments and soil.
Vertical axis: elevation [m a.s.l]; horizontal axis: profile meter; color encoded scale: v_s [m/s]; vertical exaggeration: 2:1; gray diamonds: receiver positions; red triangles: source positions; magenta crosses: positions of determined velocity values. The station spacing is 2 m, profile meter 0 = profile station number 00, profile meter 96 = profile station 48.

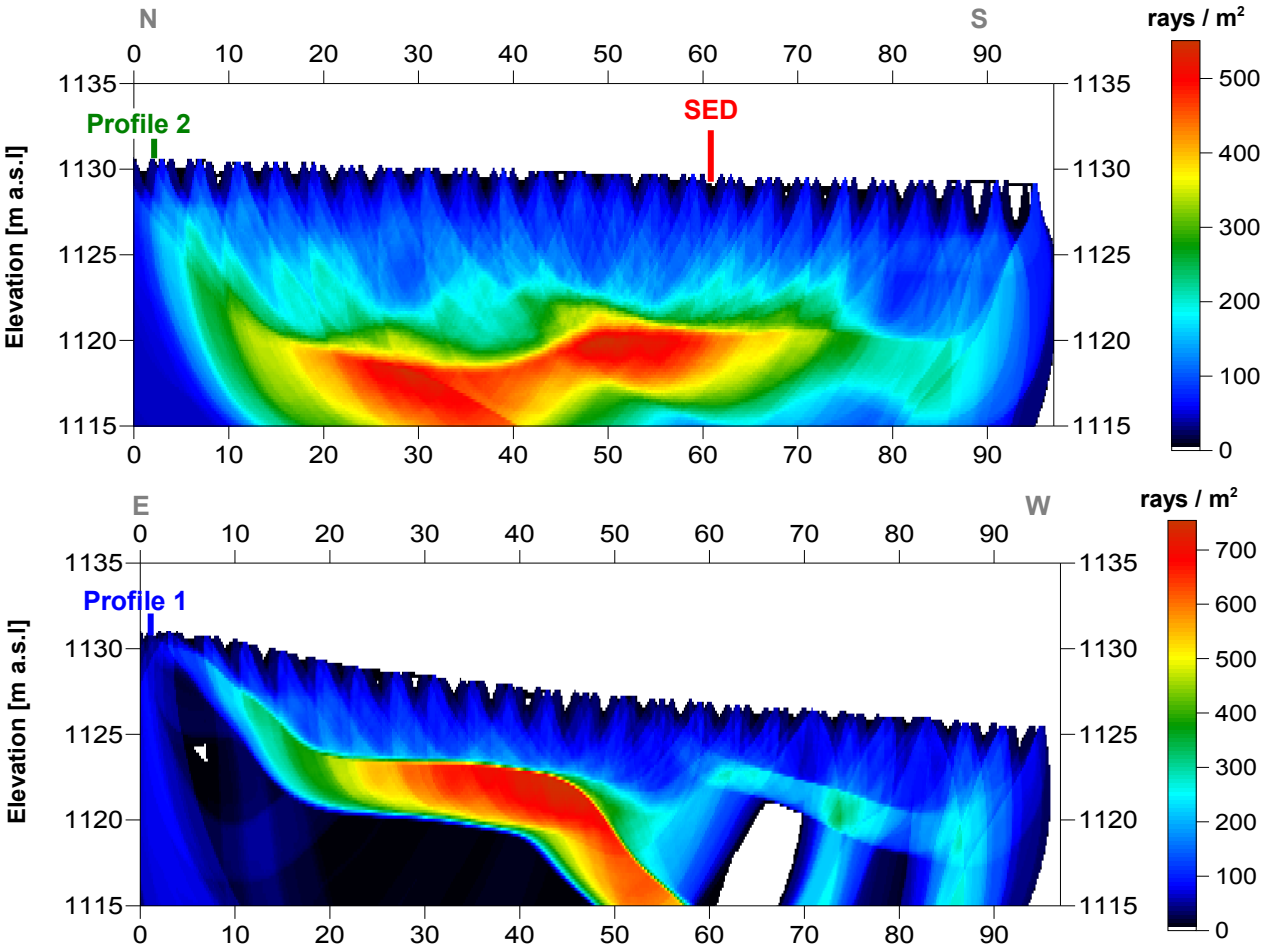

Fig. 3.2f: Shear wave ray path density along the seismic line 09SN_08GIMEL-S1 (top) and -S2 (bottom). Red/white colors indicate high velocity contrasts (usually at the bedrock surface), blue/black colors denote low coverage areas. Vertical axis: elevation [m a.s.l]; horizontal axis: profile meter; color encoded scale: ray paths per m2; vertical exaggeration: 2:1. The station spacing is 2 m, profile meter 0 = profile station 00, profile meter 96 = profile station 48.

Depth [m]	Vs [m/s]
0.0	247
1.8	640
3.6	1126
5.3	1348
7.1	1603
8.9	1949
10.7	2285
12.5	2448
14.2	2503
16.0	2525
17.8	2536
19.6	2322
21.4	2398
23.1	2548
24.9	2788

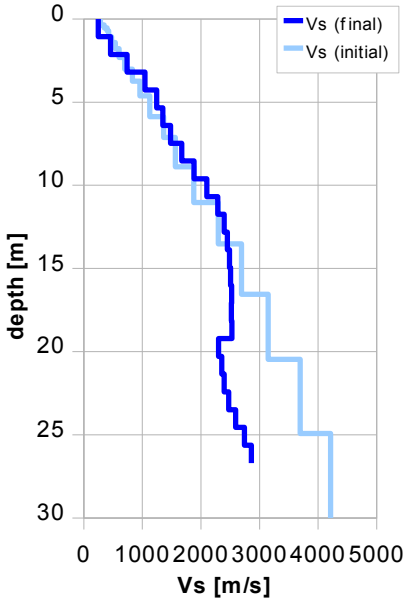

Tab. 3.2b: Final 1D s-wave velocity model derived from real data of line 09SN_08GIMEL-S1 (horizontal average of all values). The calculated values of the initial 1D s-wave velocity model are given in Tab. 3.2a.

Depth [m]	Vs [m/s]
0.0	383
1.8	779
3.5	1146
5.3	1623
7.0	1820
8.8	1606
10.5	1722
12.3	1938
13.9	2192
15.6	2452
17.4	2764
19.1	3032
20.9	3317
22.6	3617
24.4	3900
26.0	4176

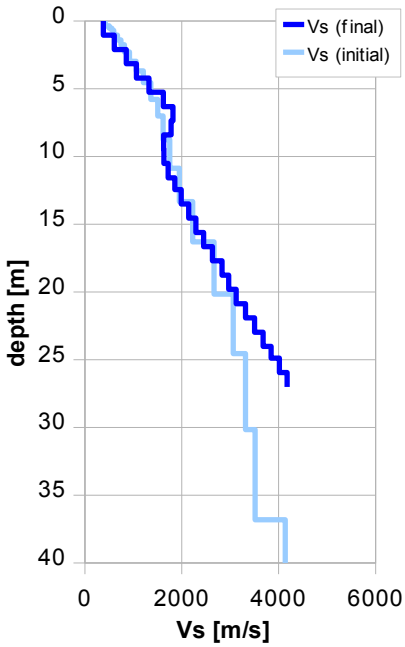

Tab. 3.2c: Final 1D s-wave velocity model derived from real data of line 09SN_08GIMEL-S2 (horizontal average of all values). The calculated values of the initial 1D s-wave velocity model are given in Tab. 3.2a.

3.3 MASW Processing

3.3.1 Reformatting and field geometry assignment

The data preparation steps for the dispersion analysis include

- the assignment of the field acquisition geometry
- the selection of suitable offset ranges (=arrays) between 10 m and 50 m for dispersion, and the splitting of the field records in forward and reverse shooting direction data sets
- the reformatting of the data into the specific KGS format

X - - ... - - o-o-o-...-o-o-o (forward shooting or so-called PLUS direction)
respectively
o-o-o-...-o-o-o - - ... - - X (reverse shooting or so-called MINUS direction).

where **X** = shot position
o = receiver station
- = 1.0 m offset

The active array used at SED-station GIMEL are the receiver station in the shot offset range between 10 and 50 m.

3.3.2 Calculating the dispersion image (overtone)

The result of dispersion analysis is the color encoded acoustic energy distribution in the phase velocity - frequency plane (see Fig. 3.3a and b).

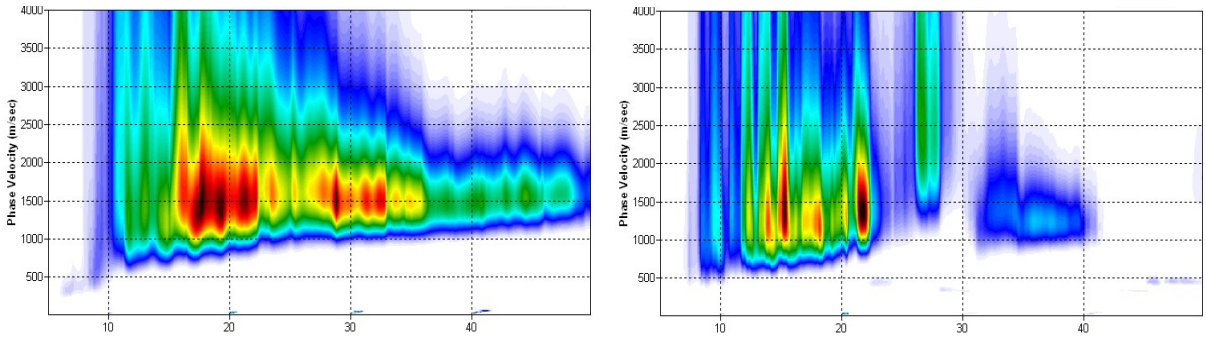

Fig. 3.3a: Dispersion image of a good to high quality data (left) as found on more than 90 % and of fair quality data (right) of midpoint station 76 representing about less than 10 % of the MASW dataset of site GIMEL.
Horizontal axis: frequency from 5 to 50 Hz; vertical axis: phase velocity from 0 to 4000 m/s; color code: colors from white (no energy) to blue - green - yellow - red - black point to increasing energy amplitude values.

3.3.3 Analysis of the dispersion image

In the dispersion graphs as calculated in section 3.3.2 above, the curves joining the amplitude peaks of the fundamental modes are determined either by subjective inspection or in a semi-automated manner. On datasets with poorly defined amplitude peaks or with a highly irregular alignment of the peaks, the danger of obtaining improbable or wrong results is real and can only be mitigated by the processing experience and the a-priori knowledge of the geological setting by the geophysicist responsible for the data evaluation.

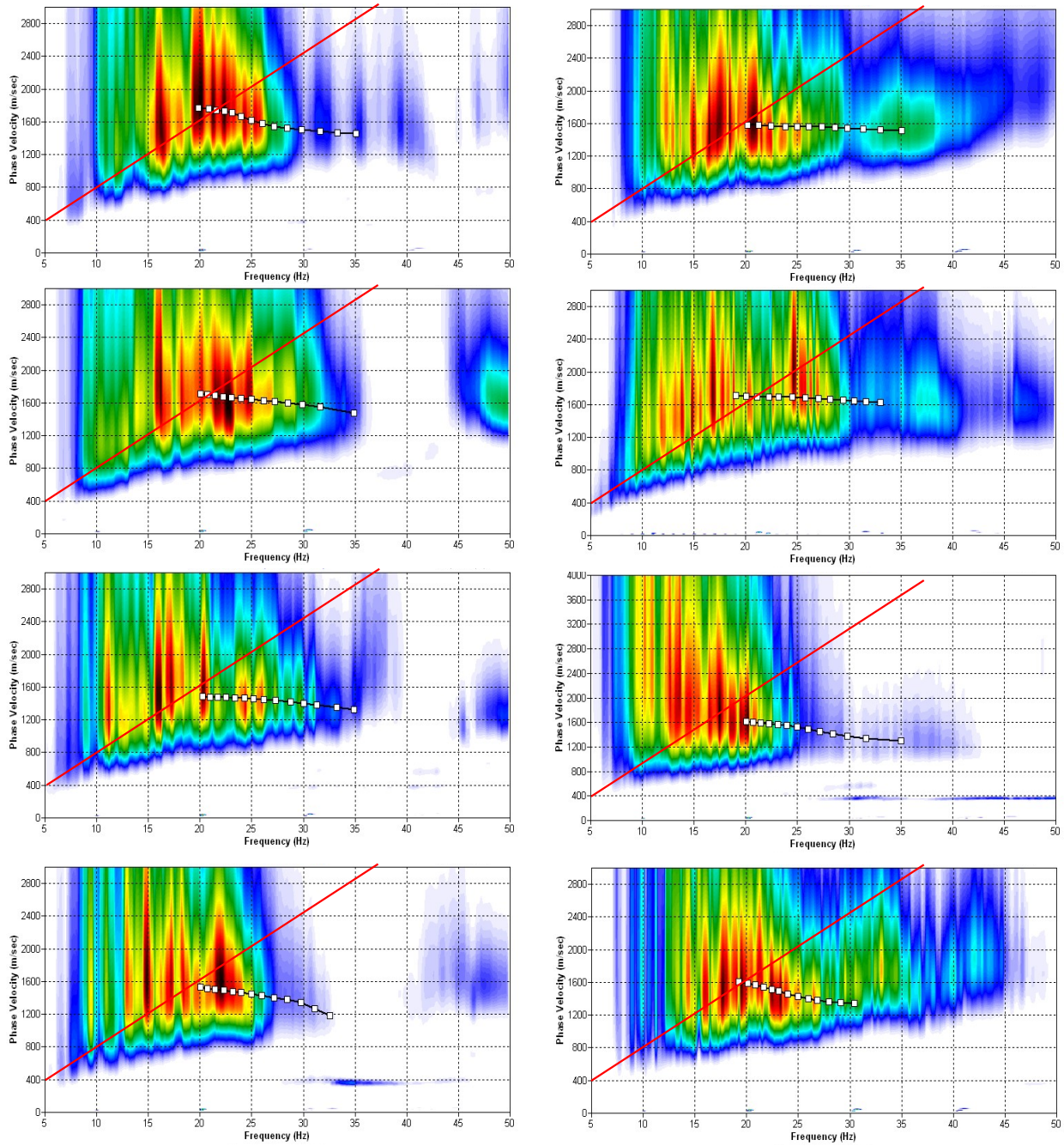

Fig. 3.3b: The manually picked dispersion images used for the derivation of the shear wave velocity section on line 09SN_08GIMEL-M1. The dispersion curves (squares) are determined by linking the peaks of high energy. Note that 'higher modes' may at times produce higher energy peaks than the fundamental mode required for the analysis.
dotted fine line: signal-noise ratio for the designated f-v_{ph} – value.
red line: high resolution beam-forming curve for v_{max}.
1st row: left: station 25 @ PLUS direction; right: station 20 @ MINUS direction
2nd row: left: station 39 @ PLUS direction; right: station 38 @ MINUS direction
3rd row: left: station 55 @ PLUS direction; right: station 57 @ MINUS direction
4th row: left: station 73 @ PLUS direction; right: station 73 @ MINUS direction

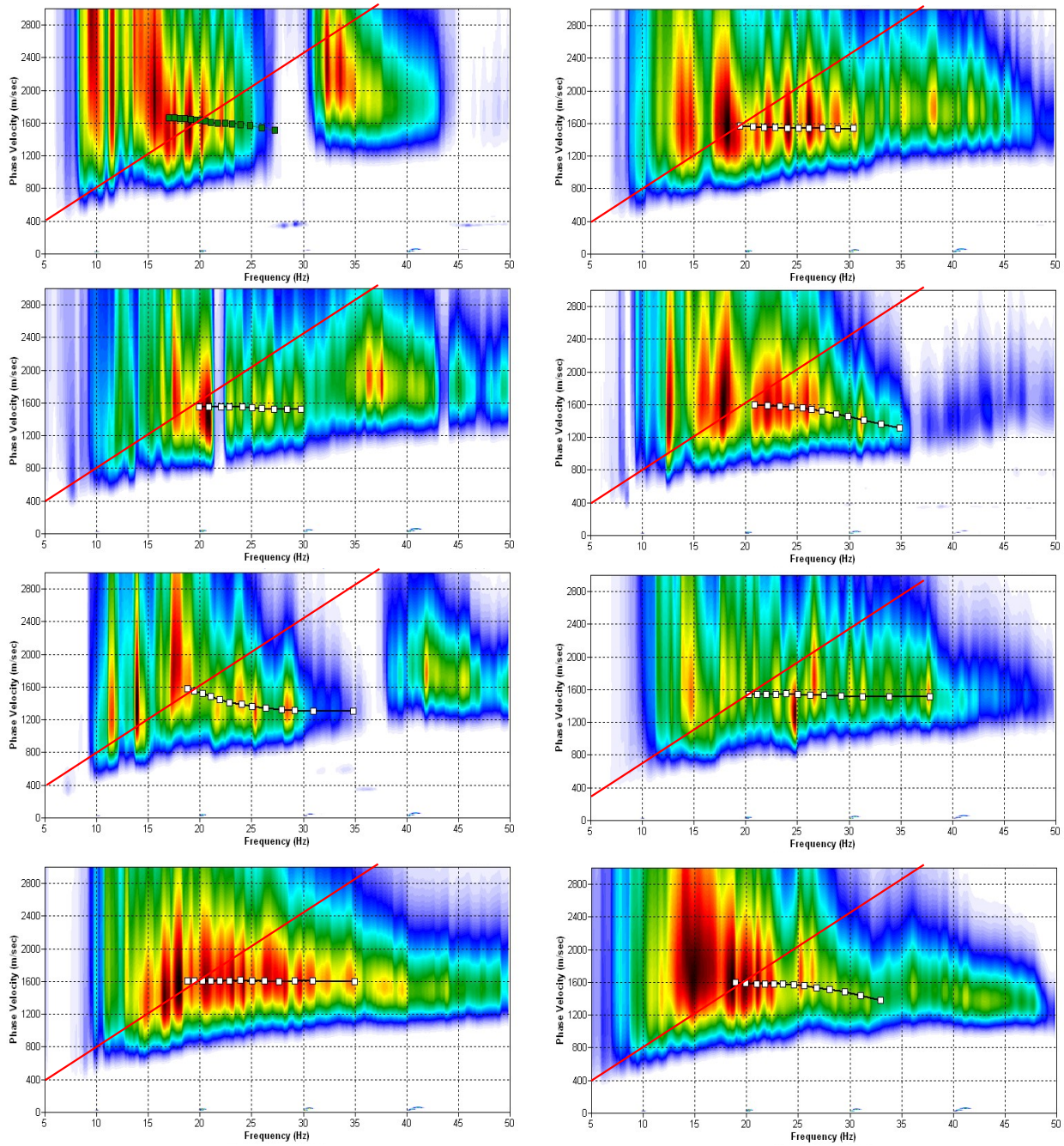

Fig. 3.3c: The manually picked dispersion images used for the derivation of the shear wave velocity section on line 09SN_08GIMEL-M2. The dispersion curves (squares) are determined by linking the peaks of high energy. Note that 'higher modes' may at times produce higher energy peaks than the fundamental mode required for the analysis.
dotted fine line: signal-noise ratio for the designated f-v_{ph} – value.
red line: high resolution beam-forming curve for v_{max}.
1st row: left: station 23 @ PLUS direction; right: station 23 @ MINUS direction
2nd row: left: station 37 @ PLUS direction; right: station 42 @ MINUS direction
3rd row: left: station 55 @ PLUS direction; right: station 58 @ MINUS direction
4th row: left: station 73 @ PLUS direction; right: station 76 @ MINUS direction

3.3.4 Inversion of dispersion curves resulting in a 1D shear wave velocity distribution

Inversion of the extracted dispersion curves was performed using the algorithm described by Xia et al. (1999).

The inversion process is started by setting the maximum depth (z_{max}) to be in the order of 30% of the largest wavelength for an initial model consisting of 10 layers of increasing thicknesses. For all 10 layers the Poisson's ratio is assumed to be 0.4 and the rock/soil density to be 2.0 g/cm^3. The inversion process is concluded either after twelve iterations or when the convergence condition of a RMS-error of less than 3 m/s (phase velocity) is met.

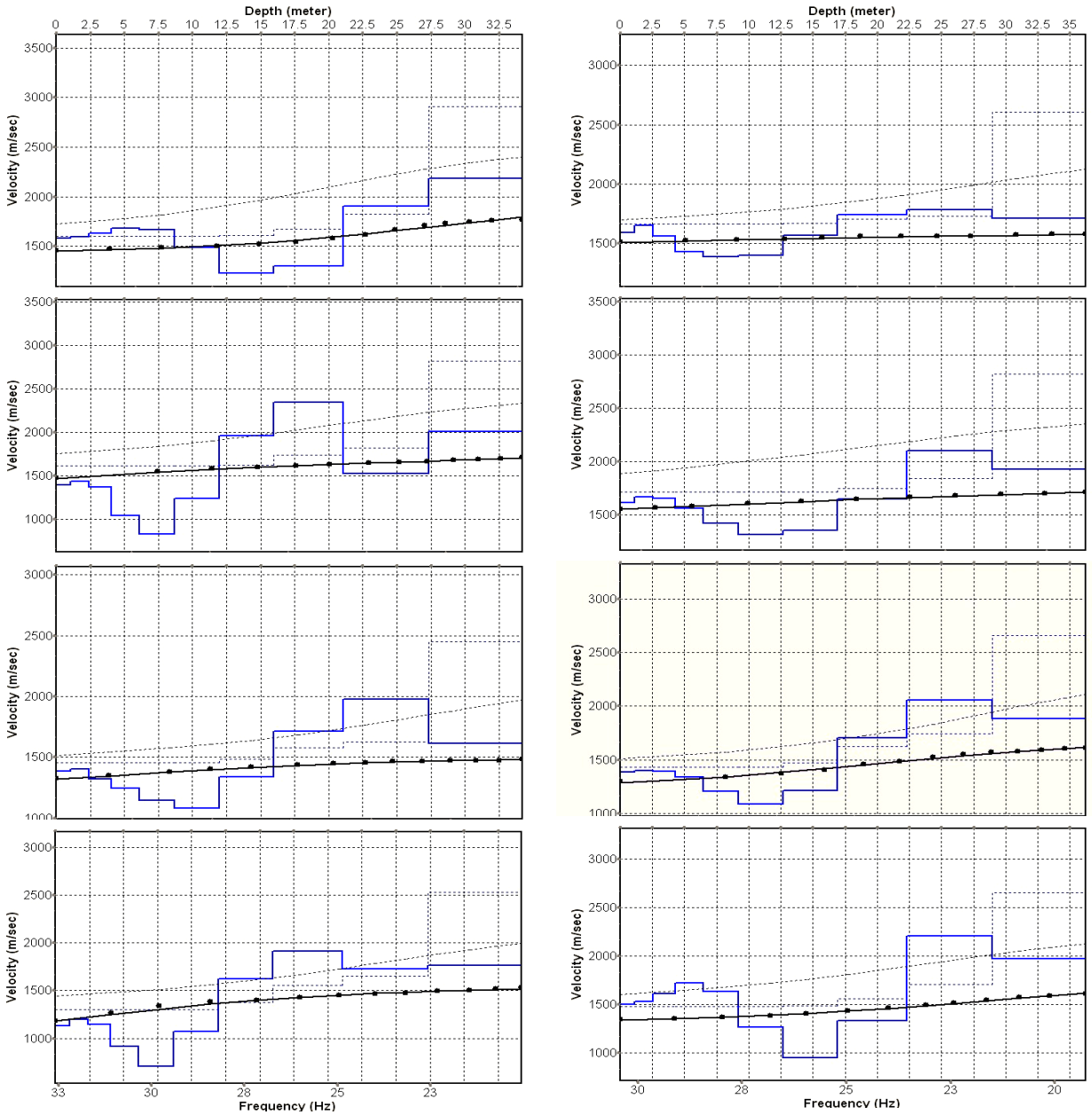

Fig. 3.3d: Inversion results of dispersion curves of dataset at line 09SN_08GIMEL-M1.
***brown**: Inversion of dispersion curve (dots) resp. of the modeled dispersion curve (dotted line: initial model; continuous line: end model). Horizontal axis: frequency Hz, vertical axis: v_s.*
***blue**: 10-layer-model (dotted: initial model, continuous line: final model). Horizontal axis: depth, vertical axis: phase velocity resp. v_s).*
1st row: left: station 25 @ PLUS direction; right: station 20 @ MINUS direction
2nd row: left: station 39 @ PLUS direction; right: station 38 @ MINUS direction
3rd row: left: station 55 @ PLUS direction; right: station 57 @ MINUS direction
4th row: left: station 73 @ PLUS direction; right: station 73 @ MINUS direction

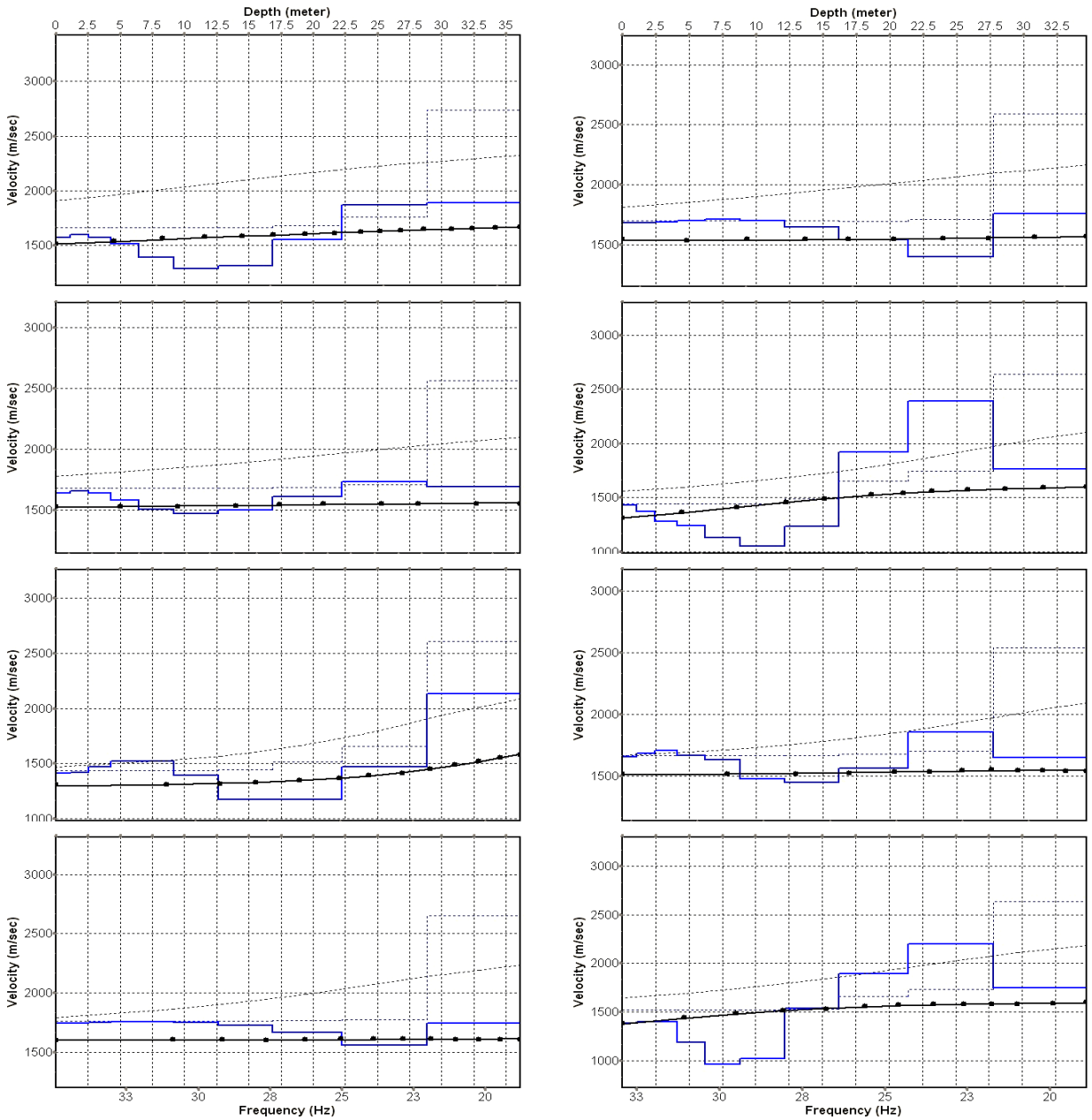

Fig. 3.3e: Inversion results of dispersion curves of dataset at line 09SN_08GIMEL-M2.
***brown**: Inversion of dispersion curve (dots) resp. of the modeled dispersion curve (dotted line: initial model; continuous line: end model). Horizontal axis: frequency Hz, vertical axis: v_s.*
***blue**: 10-layer-model (dotted: initial model, continuous line: final model). Horizontal axis: depth, vertical axis: phase velocity resp. v_S).*
1st row: left: station 23 @ PLUS direction; right: station 23 @ MINUS direction
2nd row: left: station 37 @ PLUS direction; right: station 42 @ MINUS direction
3rd row: left: station 55 @ PLUS direction; right: station 58 @ MINUS direction
4th row: left: station 73 @ PLUS direction; right: station 76 @ MINUS direction

Dispersion analyses of records with longer receiver arrays should – by theory – increase the investigation depth. At GIMEL, with both lines and both directions, MASW processing with the maximal array length of 96 m doesn't improve the results (Fig. 3.3f and 3.3g).

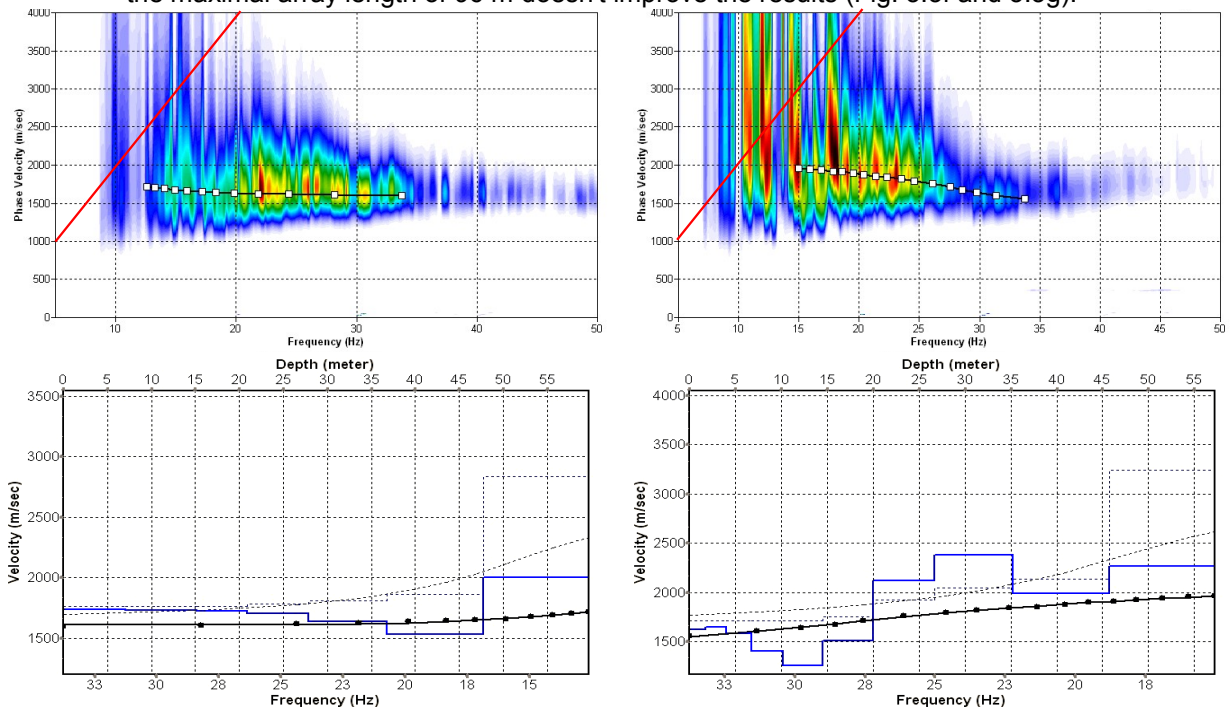

Fig. 3.3f: Top: dispersion images of over-all arrays (10...106 m offset) of line 09SN_08GIMEL-M1 in PLUS (left) and MINUS (right) direction; dotted fine line: signal-noise ratio for the designated f-v_{ph}-value. Red line: high resolution beam-forming curve for v_{max}.
*Below: The two respective inversion results; **brown**: inversion of dispersion curve; **blue**: 10-layer-model. Horizontal axis: depth, vertical axis: phase velocity resp. v_s.*

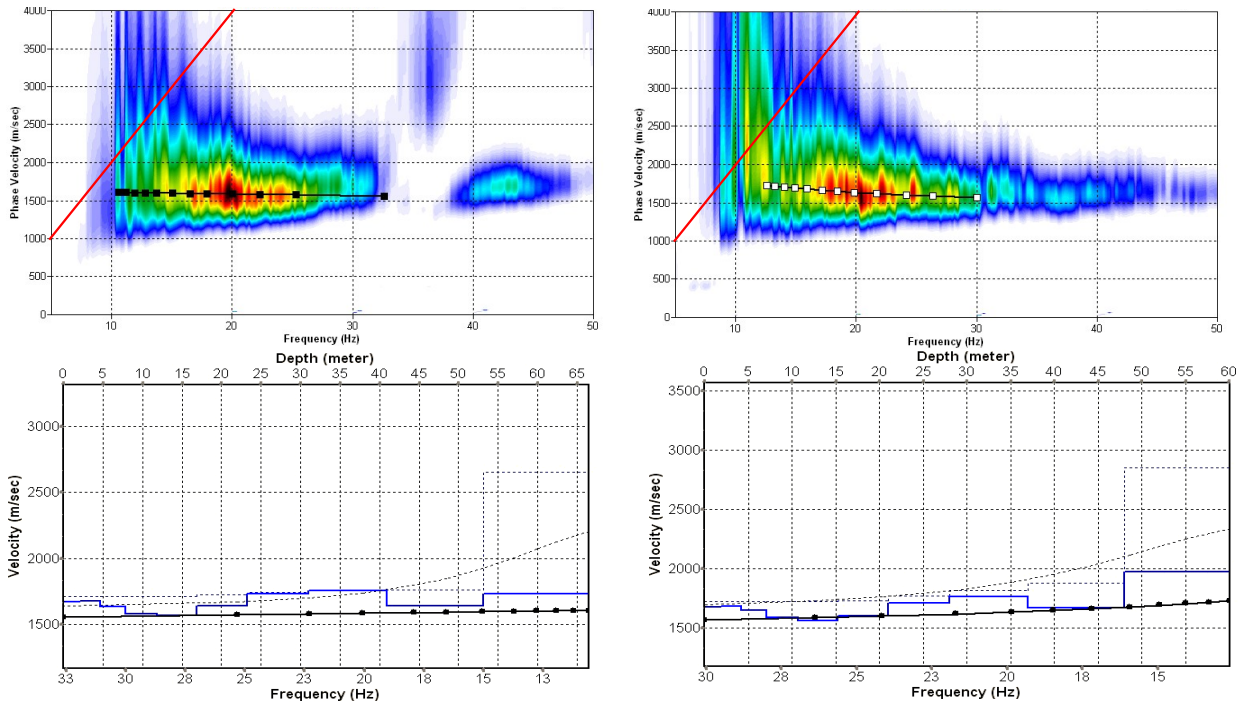

Fig. 3.3g: Top: dispersion images of over-all arrays (10...106 m offset) of line 09SN_08GIMEL-M2 in PLUS (left) and MINUS (right) direction; dotted fine line: signal-noise ratio for the designated f-v_{ph} – value. Red line: high resolution beam-forming curve for v_{max}.
*Below: The two respective inversion results; **brown**: inversion of dispersion curve; **blue**: 10-layer-model. Horizontal axis: depth, vertical axis: phase velocity resp. v_s.*

3.3.5 Gridding and plotting of 2D v_s-velocity field

By assembling the 1D v_s - depth functions of all stations the final 2D v_s-field is derived using a Kriging gridding procedure as portrayed in Fig. 3.3h and 3.3i below:

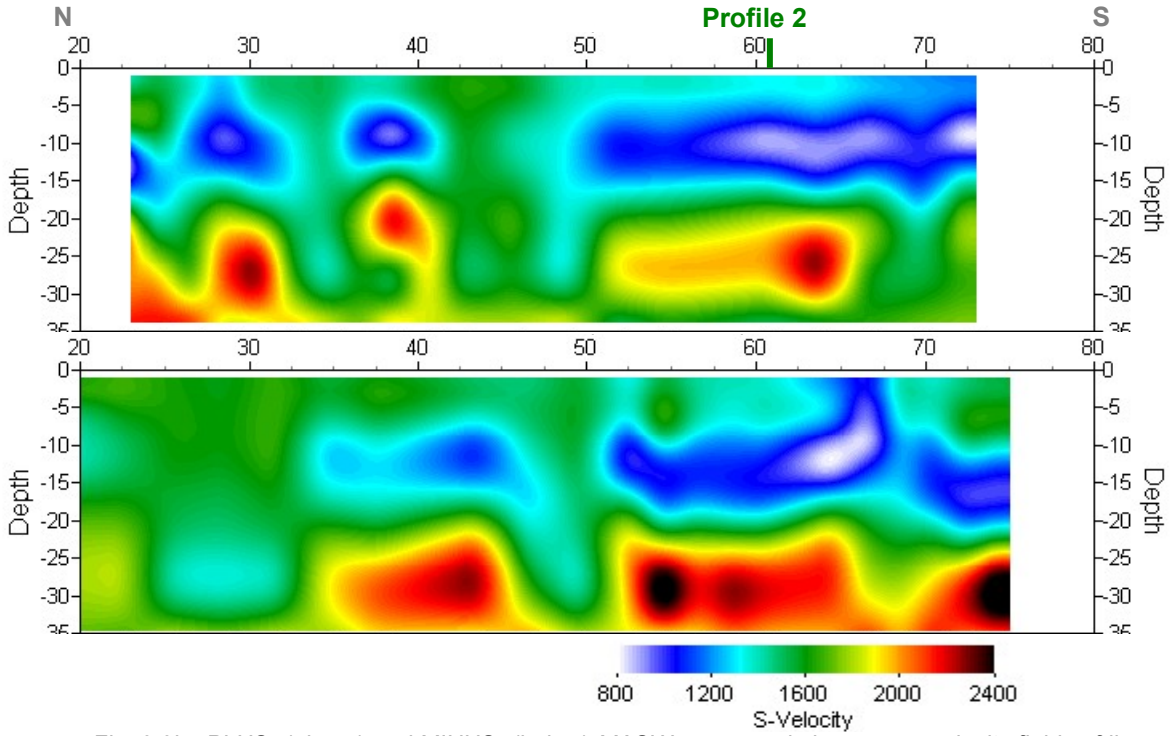

Fig. 3.3h: PLUS- (above) and MINUS- (below)-MASW-processed shear wave velocity fields of line 09SN_08GIMEL-M1. Station spacing is 1 m.

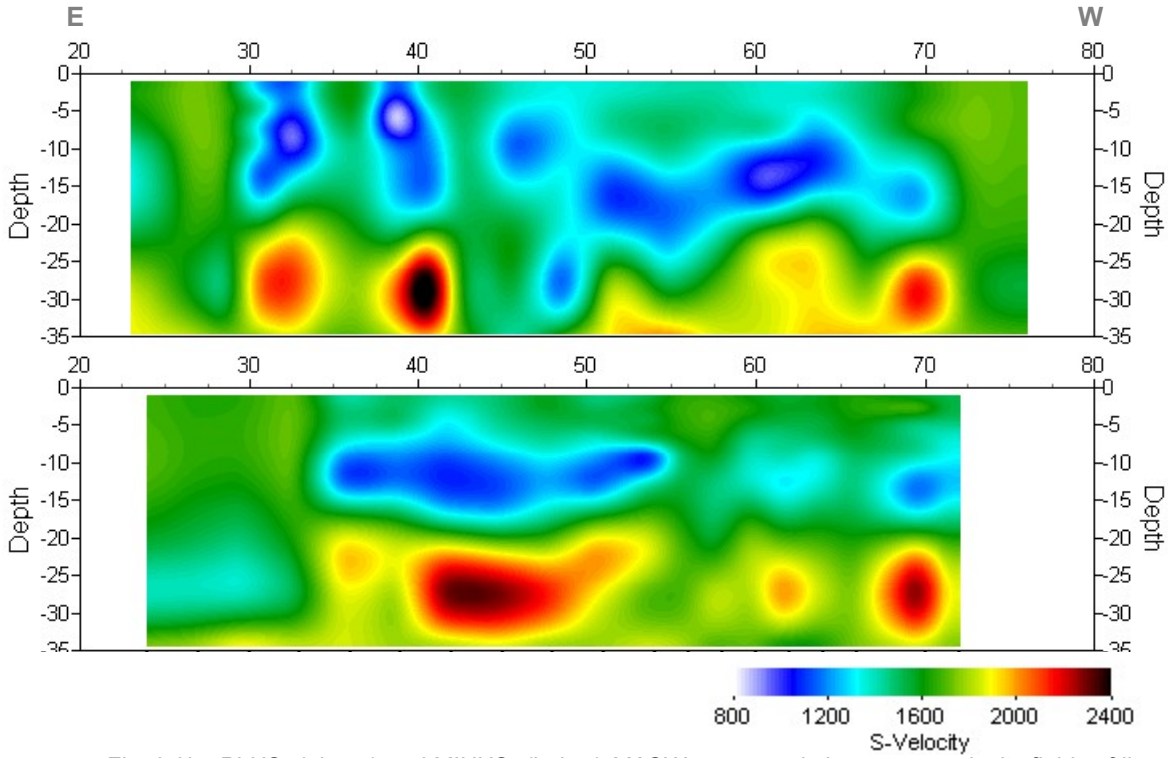

Fig. 3.3i: PLUS- (above) and MINUS- (below)-MASW-processed shear wave velocity fields of line 09SN_08GIMEL-M2. Station spacing is 1 m.

3.3.6 Calculation of the average shear wave velocity

In order to calculate a representative shear wave velocity-depth function of line 09SN_08GIMEL-M1 at the SED station, all computed 1D-v_s-depth functions are averaged (non-weighted mean values). The resulting v_s-depth-function is shown in Tab. 3.3a.

Depth [m]	Vs- [m/s]	Vs+ [m/s]	Vs [m/s]
0.0	1469	1394	1432
2.5	1489	1420	1454
4.2	1491	1395	1443
6.3	1451	1298	1374
9.0	1346	1175	1260
12.3	1241	1174	1208
16.5	1313	1404	1359
21.7	1635	1724	1679
28.2	1951	1776	1863
35.2	1908	1813	1861

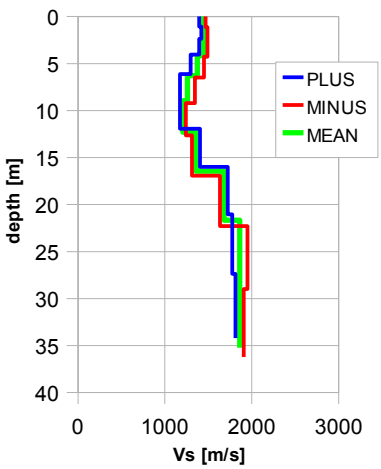

Tab. 3.3a: Averaged vs - depth function of line 09SN_08GIMEL-M1 at the SED station Gimel. Blue line: MASW-'PLUS' processing, red line: MASW-'MINUS' processing; green line: average of PLUS- and MINUS-functions.

In order to calculate an representative shear wave velocity-depth function of line 09SN_08GIMEL-M2 at the SED station, all computed 1D-v_s-depth functions are averaged (non-weighted mean values). The resulting v_s-depth-function is shown in Tab. 3.3b.

Depth [m]	Vs- [m/s]	Vs+ [m/s]	Vs [m/s]
0.0	1328	1443	1386
3.0	1357	1485	1421
5.0	1356	1421	1388
7.6	1285	1290	1287
10.8	1164	1217	1190
14.8	1148	1266	1207
19.9	1391	1564	1478
26.2	1717	1983	1850
34.0	1764	2252	2008
42.5	2307	2228	2268

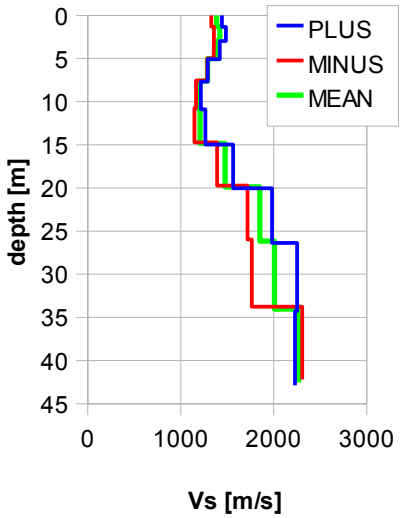

Tab. 3.3b: Averaged v_s - depth function of line 09SN_08GIMEL-M2 at the SED station GIMEL. Blue line: MASW-'PLUS' processing, red line: MASW-'MINUS' processing; green line: average of PLUS- and MINUS-functions.

The inversion of the four 100 m-array dispersion curves data (10 to 106 m offset, see Fig. 3.3f and 3.3g) are given in Tab. 3.3c. These values are complemented with the values derived of the 40 m-arrays analyses (Tab. 3.3a and 3.3b).

	100 m array							40 m array					
depth	m1+	m1-	m2+	m2-	m1	m2	m	depth	m1	depth	m2	depth	m
1.9	1736	1624	1673	1675	1680	1678	1678	0.0	1432	0.0	1386	0.0	1409
4.2	1739	1644	1676	1683	1691	1661	1686	2.5	1454	3.0	1421	2.7	1438
7.2	1734	1580	1631	1646	1657	1595	1649	4.2	1443	5.0	1388	4.6	1416
10.9	1731	1403	1577	1590	1567	1589	1570	6.3	1374	7.6	1287	6.9	1331
15.5	1729	1254	1567	1559	1491	1639	1517	9.0	1260	10.8	1190	9.9	1225
21.3	1726	1507	1641	1601	1617	1656	1625	12.3	1208	14.8	1207	13.6	1207
28.5	1707	2121	1729	1710	1914	1852	1852	16.5	1359	19.9	1478	18.2	1418
37.5	1640	2383	1753	1763	2011	1753	1925	21.7	1679	26.2	1850	23.9	1765
48.7	1533	1991	1639	1670	1762	1639	1721	28.2	1863	34.0	2008	31.1	1936
60.9	1999	2264	1730	1976	2132	1730	1998	35.2	1861	42.5	2268	38.9	2064

Tab. 3.3c: v_S-depth values of the four MASW-derived dispersion curves of both seismic line 09SN_08GIMEL-M1 and 09SN_08GIMEL-M2 using 100 m-arrays. The dispersion curves are shown in Fig. 3.3f and Fig 3.3g.

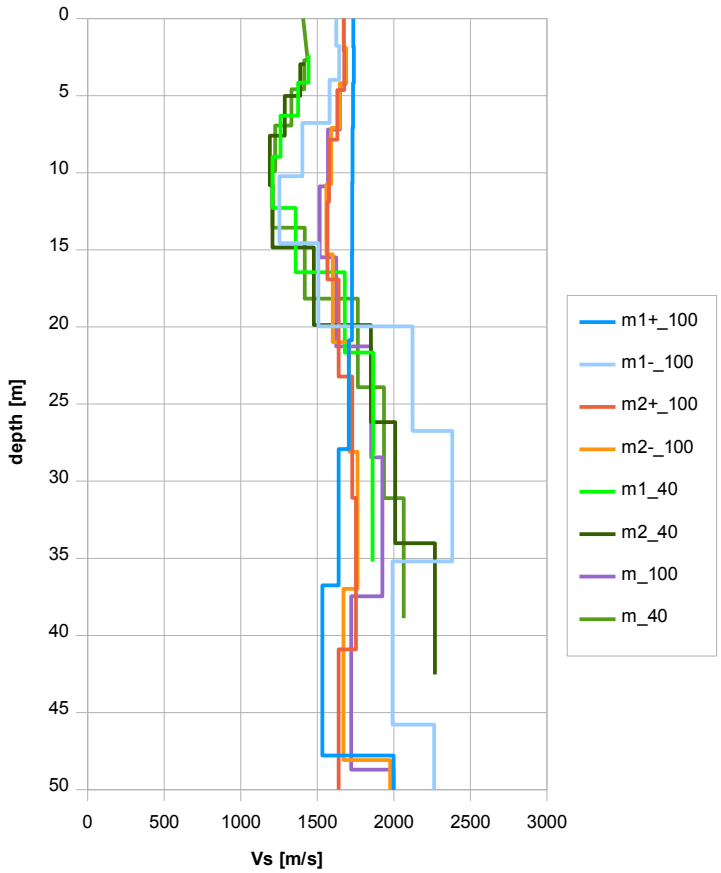

Fig. 3.3j: Comparison of the ensemble of inversion results of both lines 09SN_08GIMEL-M1 and -M2, either using the 40 m- and the 100 m-arrays.
blue lines: analyses of records of line 09SN_08GIMEL-M1
red lines: analyses of records of line 09SN_08GIMEL-M2
magenta line: mean of both 100 m-array records analyses in MINUS and PLUS direction.
green lines: vs-values of analyses of 40 m-array records.

3.3.7 Calculation of the shear wave velocity scalars $v_{s,5}$, $v_{s,10}$, ...

The parameters $v_{s,5}$, $v_{s,10}$, $v_{s,20}$, $v_{s,30}$, $v_{s,40}$, $v_{s,50}$ represent the average shear wave velocities in the depth interval between the surface and the respective depth levels and are determined from the formula

$$v_{s,n} = \frac{\sum_{i=1}^{n} d_i}{\sum_{i=1}^{n} d_i / v_{si}}$$

with:

d_i = thickness of layer i

v_{si} = corresponding shear-wave velocity.

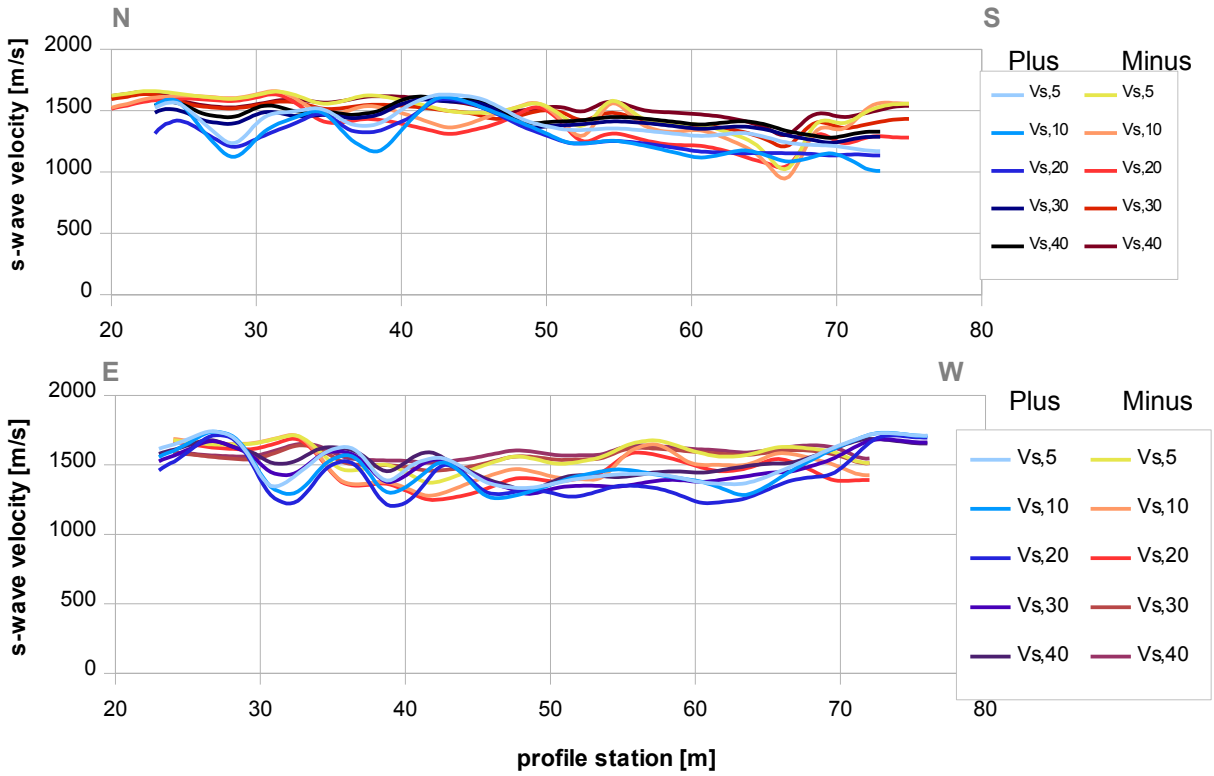

Fig. 3.3k: Graphs of the averaged vs,5...-values along the line 09SN_08GIMEL-M1 (top) resp. -M2 (bottom) for the PLUS- (blue lines) and MINUS- (red lines) directions.

The average values of the s-wave velocity model $v_{s,5}$, $v_{s,10}$, $v_{s,20}$, $v_{s,30}$, $v_{s,40}$, $v_{s,50}$, $v_{s,100}$ (= average shear wave velocity from the surface to depths of 5 m, …until 100 m) on the line segment nearest to the SED station (Tab. 3.3d) are summarized below:

	Vs,5	Vs,10	Vs,20	Vs,30	Vs,40	Vs,50
MINUS	1495	1447	1372	1467	1528	n/a
PLUS	1357	1244	1266	1407	1448	n/a
MEAN	1426	1345	1319	1437	1488	n/a

	Vs,5	Vs,10	Vs,20	Vs,30	Vs,40	Vs,50
MINUS	1569	1502	1466	1556	1586	n/a
PLUS	1455	1444	1349	1450	1514	n/a
MEAN	1512	1473	1408	1503	1550	n/a

Tab. 3.3d: The average shear wave velocities within the depth intervals from surface down to 5 m, etc.… to 50 m, calculated for the line segment with a subjectively most similar geology to the SED station (line 09SN_08GIMEL-M1, top; line 09SN_08GIMEL-M2, bottom).

3.4 Hybrid Seismic Data Processing

3.4.1 p-wave *Reflection* Seismic Processing Sequence

A) Data conditioning

A1 Reformatting and quality verification of field data
A2 Recording geometry assignment
A3 Data editing (suppression of bad / dead traces, etc.)
A4 Preliminary analysis of refraction velocities

B Filtering and deconvolution

B1 Analytical muting of refraction arrivals
B2 Amplitude recovery / amplitude equalization in time and frequency domains
B3 Predictive deconvolution parameter tests / application
B4 Determination of band limiting corner frequencies / application
B5 Optional 2-D filtering

C) Velocity analysis and stack

C1 Common Depth Point (CDP) sort
C2 Semblance velocity analysis using supergathers of 3 - 5 CDP's
C3 Optional dip move-out correction
C4 Normal Move-Out (NMO) correction and application of stretch mute
C5 Band-pass filtering
C6 CDP stack
C7 Optional coherency filtering

D) Time-depth conversion

D1 Optional spiking deconvolution
D2 Band-pass filtering
D3 Depth conversion
D4 Final display of seismic depth section with inversed polarity (non-SEG-convention)

3.4.2 The presentation of reflection seismic data

The data in a reflection seismic section are presented as an assembly of individual seismic signals at regular intervals along a seismic profile. The simplest way of representing the signals are single wiggle lines (first to the left in the illustration below). A more capturing presentation is the variable area form (second to the left). Combining these two modes results in the var-wiggle mode. Another method of data visualization is the variable density mode (second from the right).

The compressional phase of seismic signals is defined in this report as the onset of the positive amplitude excursion in black (Fig. 3.4a). Since the source signal is produced by an explosion or by an impact at the surface, the signal starts off with a compression of the ground particles. Thus the arrivals of reflection events are defined by the compressional phase.

In rare situations of velocity inversions, cases in which formation velocities are lower than in the layers above, polarity reversals of the reflected signals occur. The beginning of the reflection event would then be characterized by a dilatational phase, represented in this report as a negative amplitude excursion, i.e. in white.

The final p-wave seismic depth sections are displayed in Fig. 3.4b and 3.4c, the hybrid sections in Fig. 3.4j and -k further below.

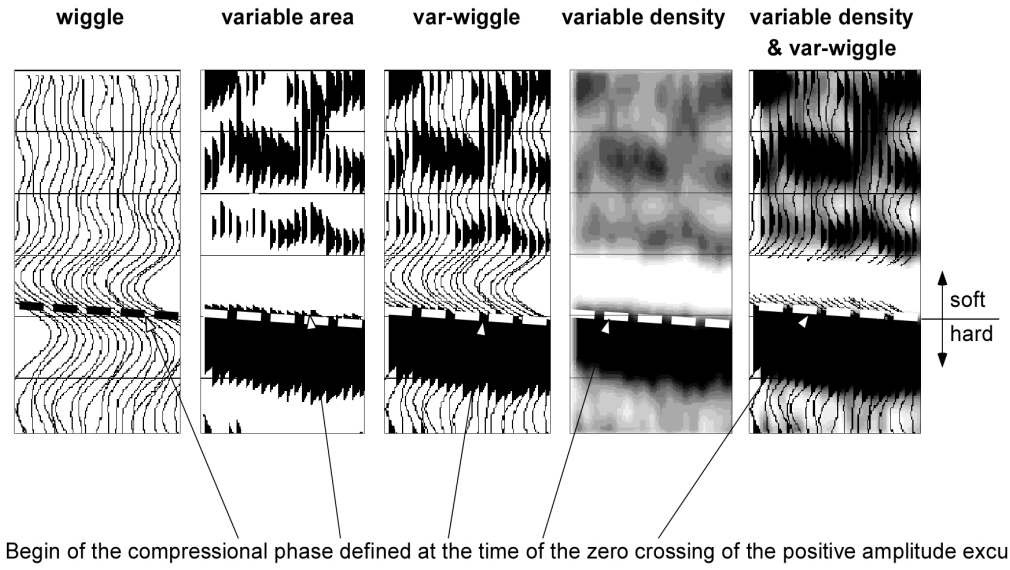

Fig. 3.4a Representation of reflection seismic data and the definition of a reflection event.

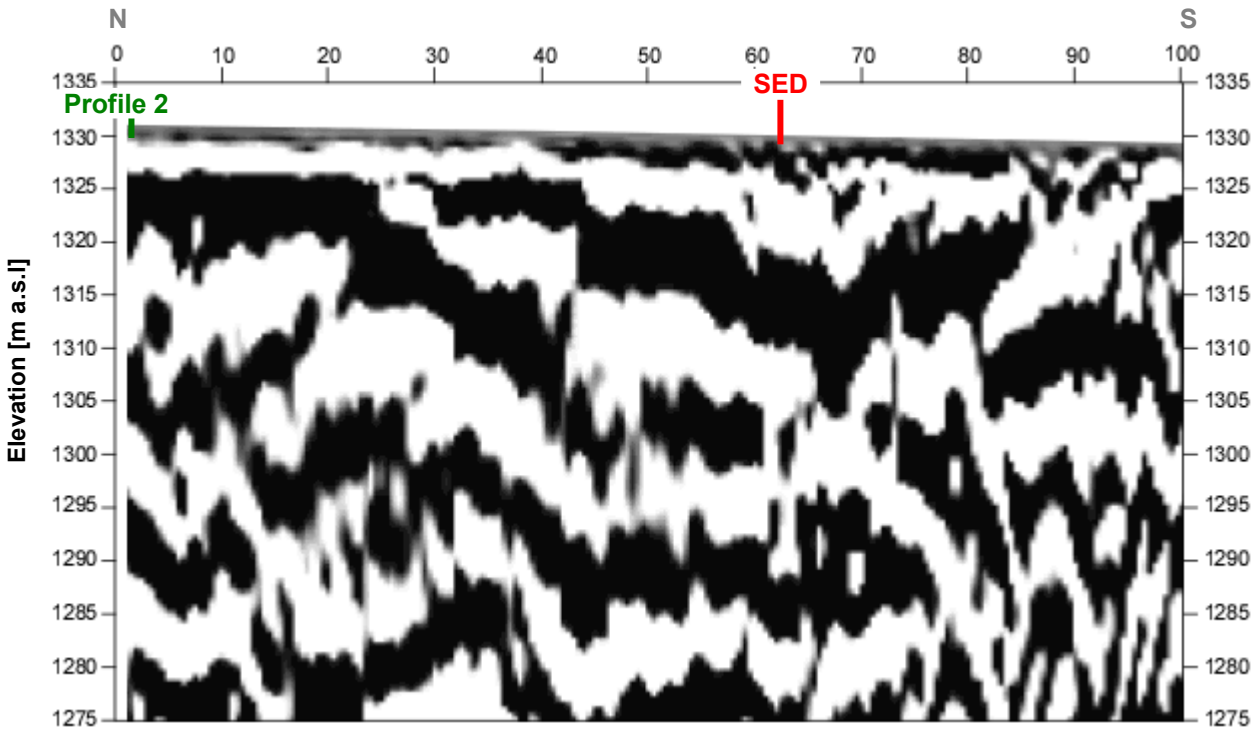

Fig. 3.4b: Seismic depth section of seismic line 09SN_08GIMEL-P1 with variable density mode presentation. Vertical axis: elevation [m a.s.l.], horizontal axis: profile meter; no vertical exaggeration. The station spacing is 1 m.

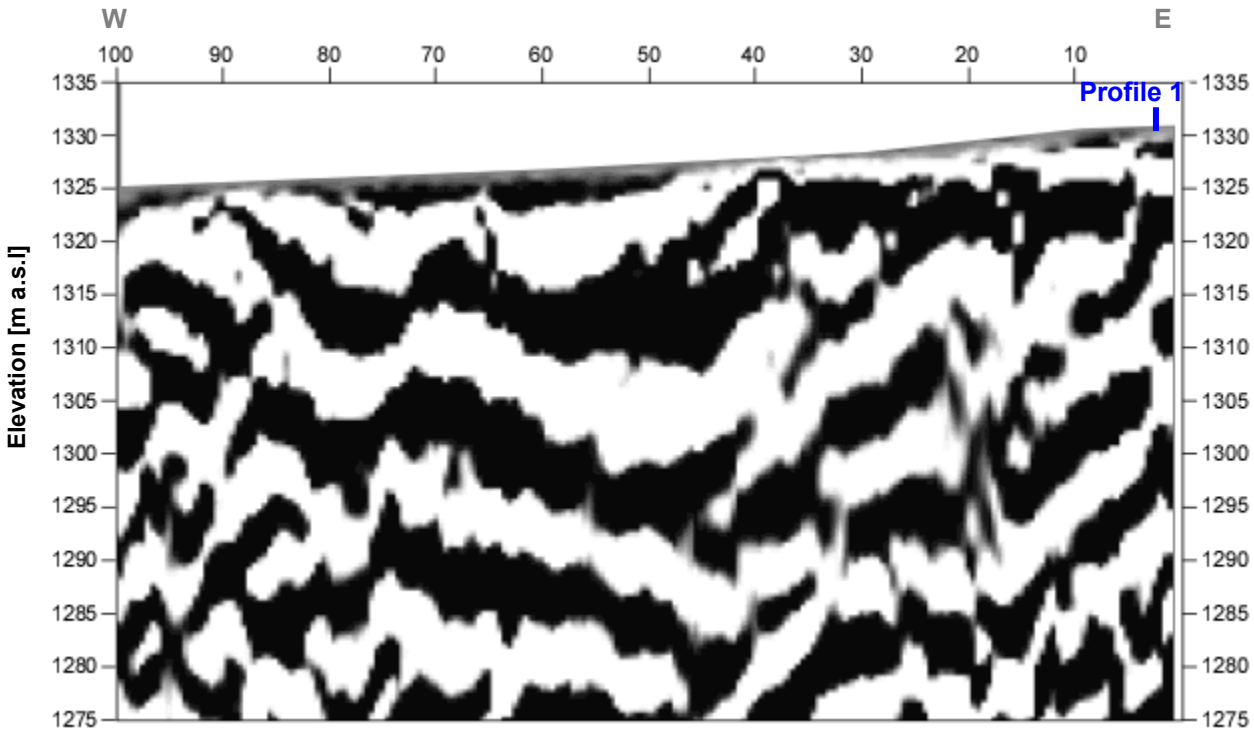

Fig. 3.4c: Seismic depth section of seismic line 09SN_108GIMEL-P1 with variable density mode presentation. Vertical axis: elevation [m a.s.l.], horizontal axis: profile meter; no vertical exaggeration. The station spacing is 1 m.

3.4.3 p-wave refraction tomography processing

The seismic p-wave refraction processing steps are analogous to those described in paragraph 3.2. For a detailed method statement and a description of the processing steps please refer to the summary report. The Figs. 3.4d to 3.4i and Tab. 3.4a illustrate the intermediate processing steps and the final result.

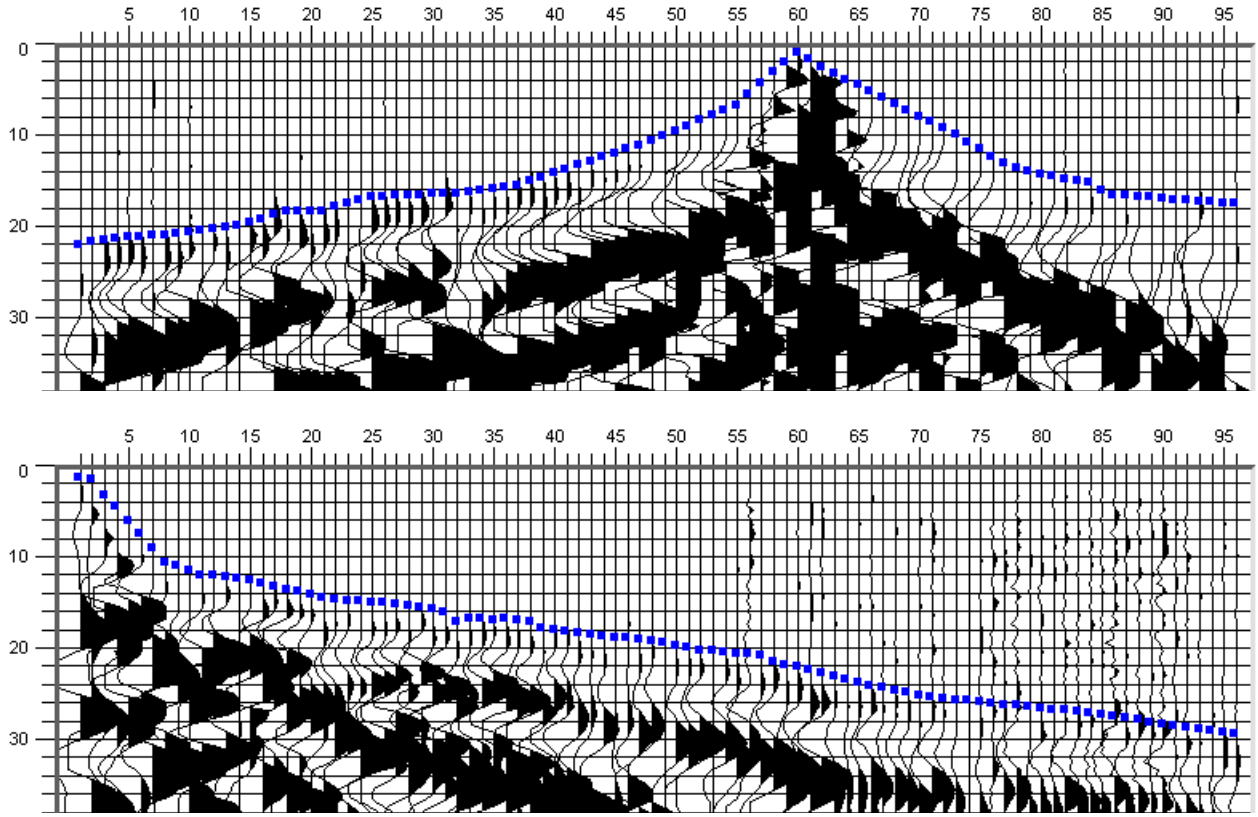

Fig. 3.4d: p-wave records of 09SN_08GIMEL-P1 (above) and -P2 (below) with positive amplitude excursions in black. Blue squares mark the manually picked first break arrival times. Vertical axis: travel time in ms, horizontal axis: station numbers spaced at 1 m.

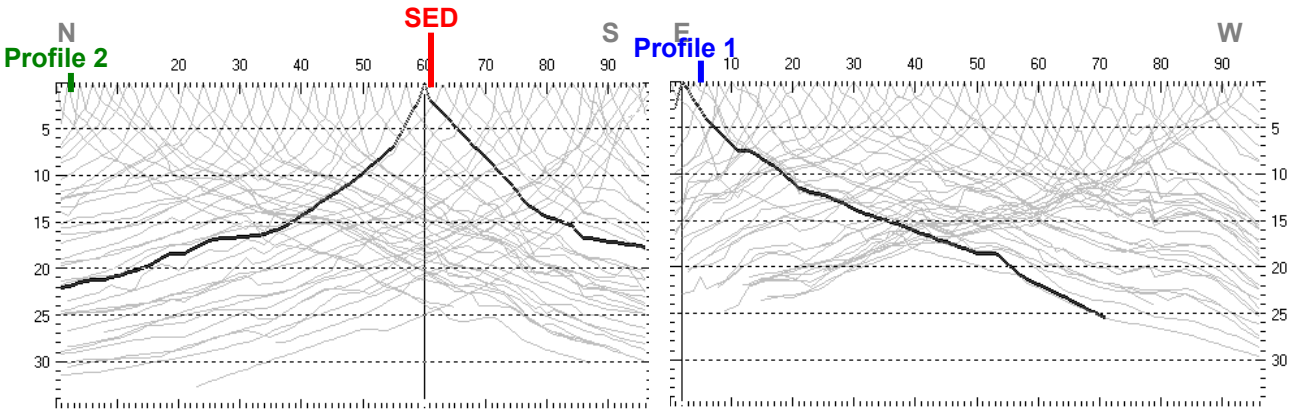

Fig. 3.4e: Travel time curves of p-wave arrival time picks of line 09SN_08GIMEL-P1 (left) and -P2 (right). Vertical axes: travel time [ms], horizontal axes: station number (= profile meter).

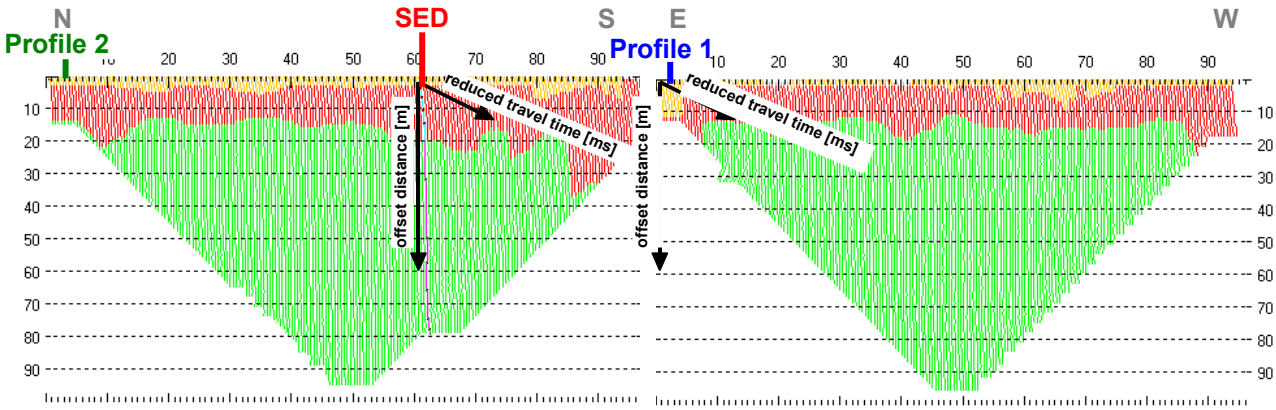

Fig. 3.4f: 3-dimensional distance-travel time diagrams at the mid-points between source points and receiver stations are instrumental when using the analytical CMP derivation of the initial velocity field. The horizontal axes are along the CMP positions and the travel time respectively, the vertical axis denotes the offset distance between source and receiver positions.

Depth [m]	Vp [m/s]
0.0	584
0.2	693
0.5	891
1.2	1178
1.7	1382
2.4	1649
3.2	1929
4.4	2311
5.9	2817
8.0	3361
10.5	3805
13.9	4034
18.3	4006
23.9	4146
31.3	3830
41.0	3674

Depth [m]	Vp [m/s]
0.0	733
0.2	733
0.5	794
0.8	870
1.2	949
1.8	1096
2.5	1325
3.5	1375
4.8	1844
6.3	2351
8.5	3060
11.3	3963
14.8	4686
19.5	4820
25.5	5102
33.5	5576

Tab. 3.4a: Initial 1D p-wave velocity model derived from real data (left: 09SN_08GIMEL-P1; right: -P2).

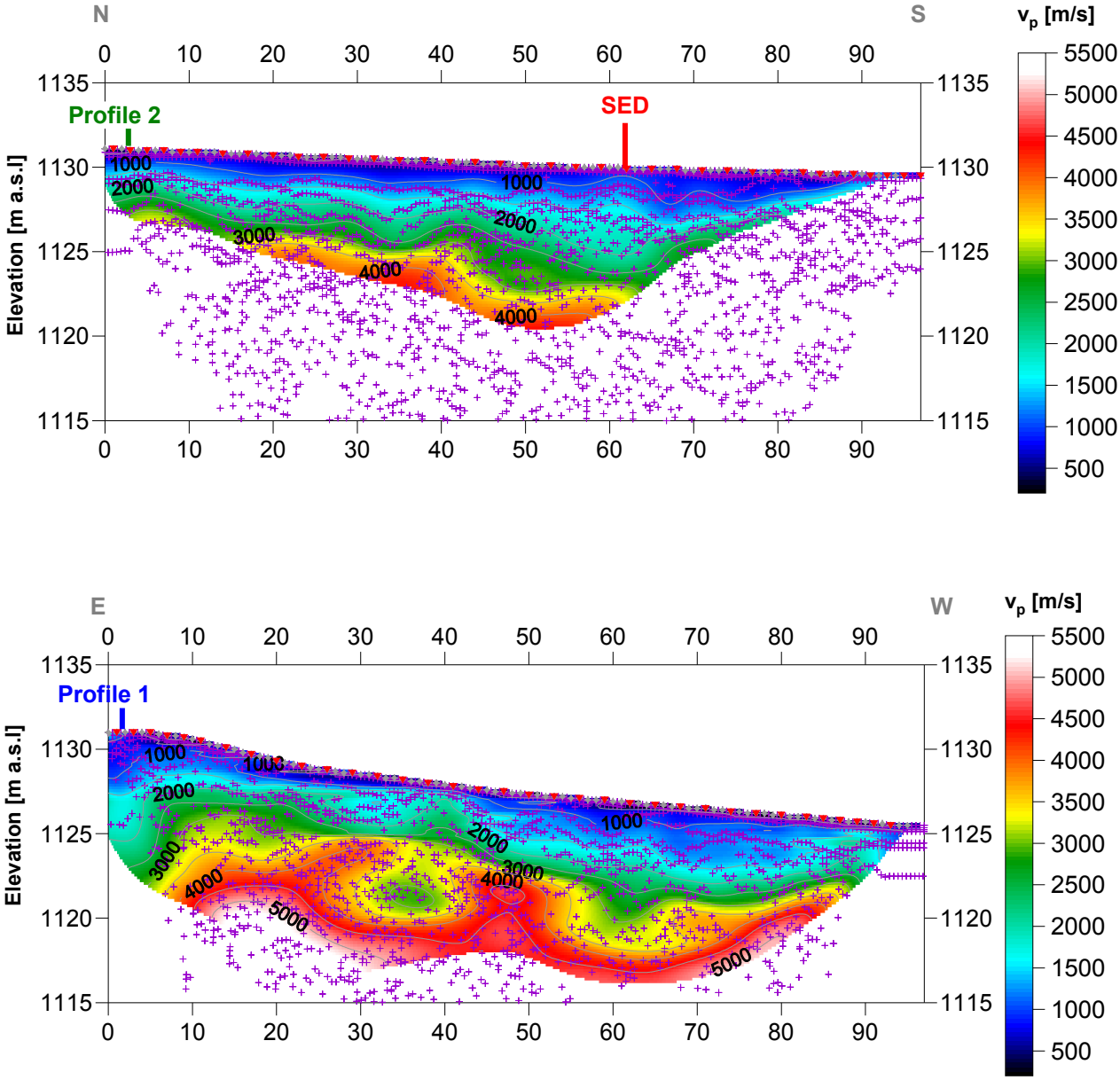

Fig. 3.4g: Compressional wave velocity field image along the seismic profiles 09SN-08GIMEL-P1 (above) and -P2 (below). Red/white colors indicate solid rock, blue/black colors unconsolidated sediments and soil. Vertical axis: elevation [m a.s.l]; horizontal axis: profile meter; color scale: v_S [m/s]; vertical exaggeration: 2:1; gray squares: receiver stations; red triangles: shot positions; magenta crosses: positions of determined velocity values.

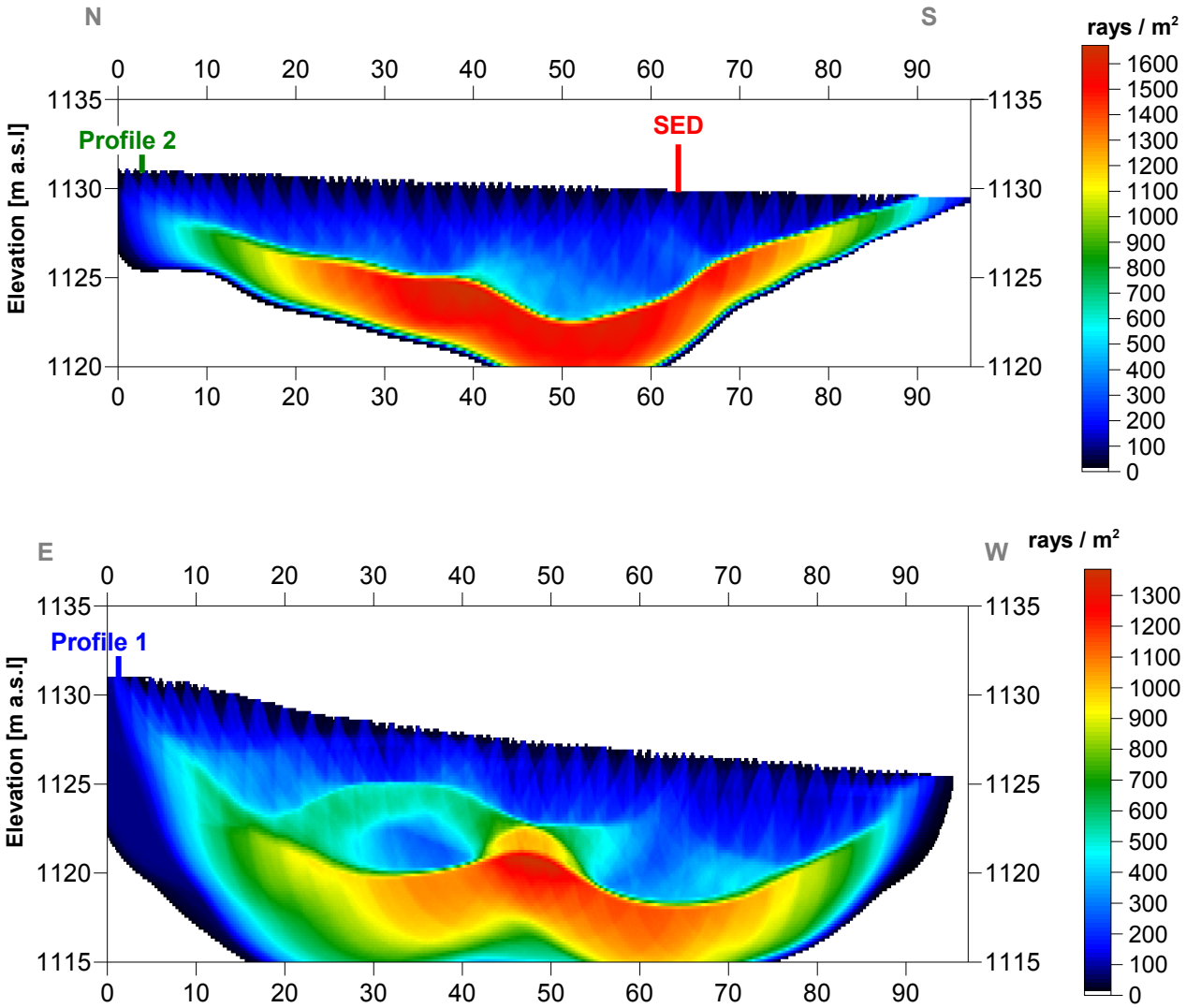

Fig. 3.4h Compressional wave subsurface ray path density along the seismic profiles 09SN_08GIMEL-P1 (above) and -P2 (below). Red/white colors indicate high velocity contrast between two layers, blue/black colors low coverage areas. Vertical axis: elevation [m a.s.l]; horizontal axis: profile meter; color scale: ray paths per m2; vertical exaggeration: 2:1.

Depth [m]	Vp [m/s]
0.0	670
0.7	852
1.2	1085
1.7	1328
2.2	1574
2.7	1822
3.2	2064
3.7	2285
4.2	2479
4.7	2609
5.2	2833
5.8	3081
6.3	3234
6.8	3362
7.3	3465
7.8	3542
8.3	3722
8.8	3965
9.3	4204

Depth [m]	Vp [m/s]
0.0	744
0.8	877
1.7	1002
2.5	981
3.3	1389
4.2	1518
5.0	1875
5.8	2202
6.7	2534
7.5	2944
8.3	3365
9.2	3662
10.0	3958
10.8	4201
11.7	4432
12.5	4746
13.3	4984

Tab. 3.4b: Final 1D p-wave velocity model derived from real data at all positions of line 09SN_08GIMEL-P1 (left) line -P2 (right) .

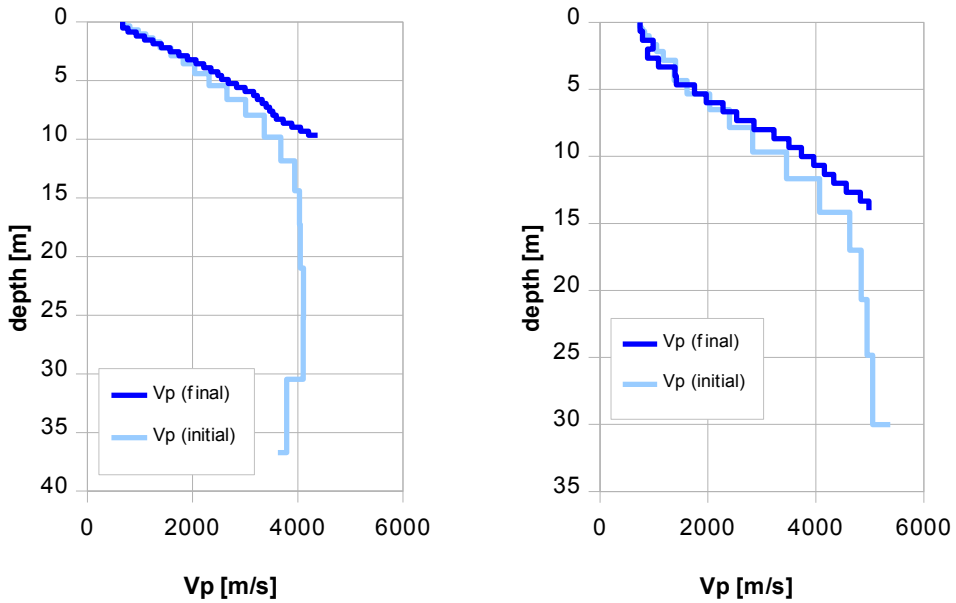

Fig. 3.4i: Final 1D p-wave velocity model derived from real data (horizontal mean) at line 09SN_08GIMEL-P1 (left) resp. -P2 (right). Initial 1D p-wave velocity model values are given in Tab. 3.4a.

3.4.4 Representation of the hybrid seismic section

The hybrid seismic section is the reflection seismic section with the superimposed p-wave velocity field. It portrays the geological structures and the p-wave velocity field, the latter being indicative for the rock / soil rigidity. The uninterpreted hybrid seismic section is portrayed in Fig. 3.4j and 3.4k below.

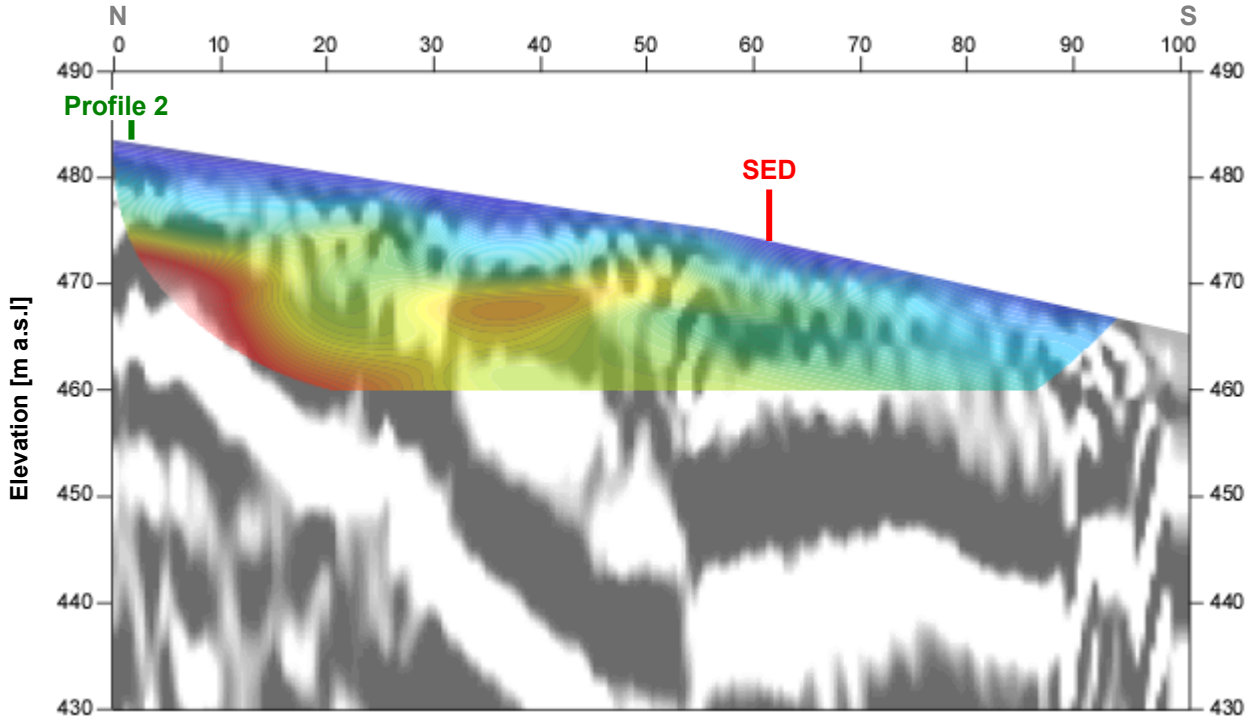

Fig. 3.4j Uninterpreted hybrid seismic section 09SN_08GIMEL-P1: superimposed onto the seismic reflection section is the color encoded p-velocity field derived by refraction tomography (no vertical exaggeration).

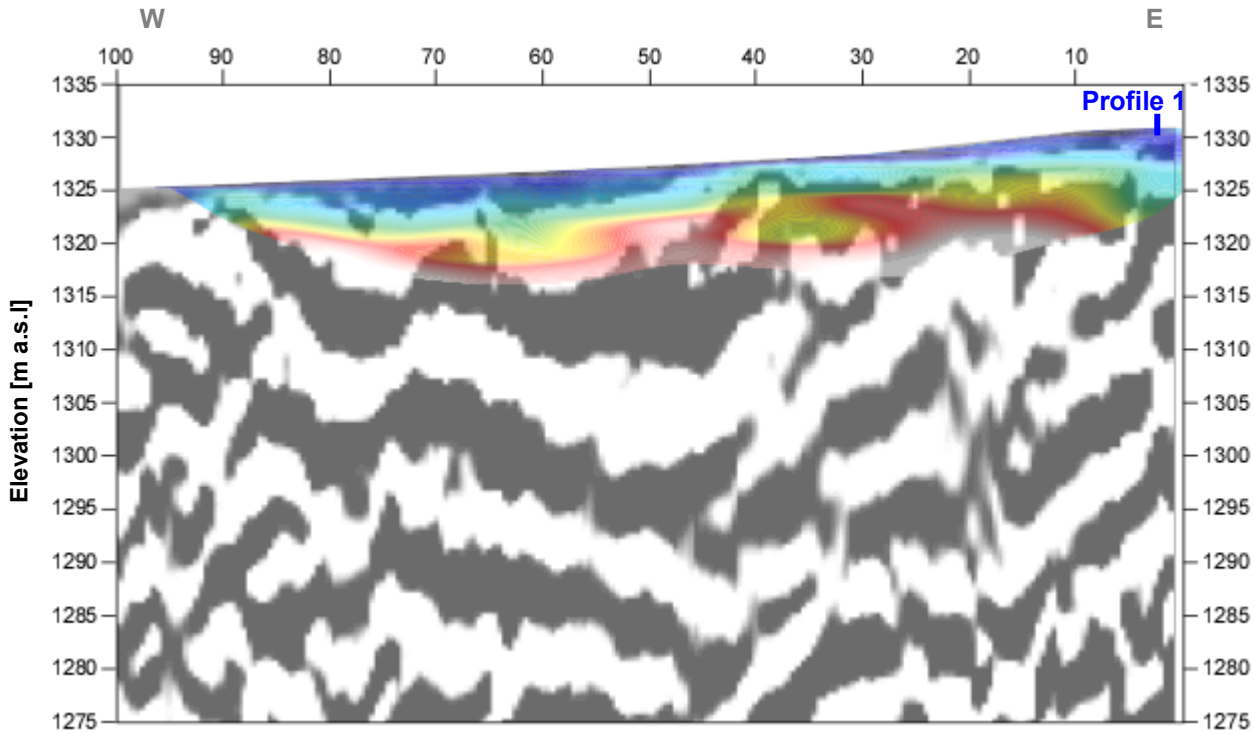

Fig. 3.4k Uninterpreted hybrid seismic section 09SN_08GIMEL-P2: superimposed onto the seismic reflection section is the color encoded p-velocity field derived by refraction tomography (no vertical exaggeration).

4 DISCUSSION OF THE RESULTS

4.1 Summary and Validation of the Results

Compressional and shear wave velocity data from refraction seismic surveys both p-wave and s-wave and also the MASW survey data of profiles 09SN_08GIMEL-1 and 09SN_08GIMEL-2 are shown in Tab. 4.1 for the uppermost 30 m. The calculated shear wave velocity $v_{s(calc)}$ in Tab. 4.1 is derived by using a theoretical v_p/v_s-ratio of $\sqrt{3}$.

Depth	Vp1	Vp2	Vs1	Vs1	Vs2	Vs2	Vs1	Vs2
	meas	meas	meas	calc	meas	calc	MASW	MASW
0	670	744	247	387	383	430	1432	1386
1			459		609		1454	1421
2	1085	987	739	627	854	570	1443	
3	1574	882	1045	909	1068	509		1388
4	2064	1389	1244	1192	1325	802	1374	
5	2479	1417	1348	1431	1623	818		1287
6	2833	1969	1480	1636	1818	1137	1260	
7	3234	2278	1670	1867	1780	1315		
8	3465	2853		2001	1626	1647	1260	1190
9	3722	3223	1884	2149	1633	1861	1208	
10	4204	3731	2100	2427		2154		
11		3958	2285		1722	2285		1207
12		4331	2395		1988	2501	1359	
13		4564	2451			2635		
14		4984	2488		2142	2877		
15			2506		2291			1478
16			2525		2452		1679	
17			2520		2635			
18			2527		2831			
19			2302		2971			
20			2354		3123			1850
21			2398		3317			
22			2473		3502		1863	
23			2591		3677			
24					3843			
25			2742		4011			
26			2860		4176			2008
27								
28							1861	
29								
30								

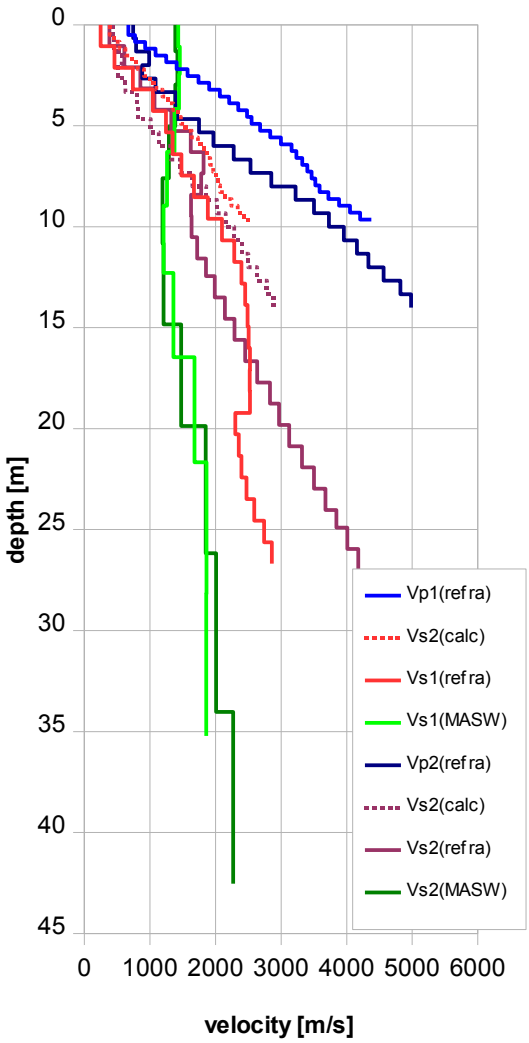

Tab. 4.1: Shear and compressional wave velocity model determined at the SED station GIMEL.

Fig. 4.1: Graphic display of shear (continuous lines) and compressional (dotted lines) wave velocities determined at the SED station. In green colors values of MASW derivation, in blue values of p-wave refraction and in red of s-wave refraction tomography.

4.2 Validation of the methods and their results

Due to methodological differences, v_s velocities derived by MASW analysis and by the refraction tomography technique may differ considerably. This is because MASW analysis cannot image small rock/soil inhomogeneities as a dispersion image with an array length of i.e. 40-m only yields one single v_s-value at each depth. On the other hand, refraction diving wave tomography results produce v_s-sections with a high lateral resolution, but fail to provide information at greater depths.

4.3 Error Estimates

The error estimates given in Tab. 4.3 below are relevant only in the context of this survey.

Surveying method	Type of result	Error estimate
v_s – refraction tomography**	v_s – velocity field image	12%
MASW only "+" or only "-" values*	v_s – velocity field image	15%
MASW (mean of "+" & "-" values)*	v_s – velocity field image	10%
v_p – refraction tomography**	v_p – velocity field image	8%
Reflection seismic surveying	Image of subsurface structures	n.a.

** MASW values in the uppermost 4 m are prone to an error of about 30 % (only one direction) resp. 20 % (mean of both directions).*
*** Refraction velocity determination in the bedrock is limited due to short receiver spreads.*

Tab. 4.3 Error estimates for the methods applied. Note that higher error estimates are to be taken into account with increasing depths.

The above error estimates are of a qualitative character only. In view of the intense fluctuations to be expected in both the lateral and vertical directions, any attempt to derive a quantitative general error estimate to be valid for the entire survey is to be considered as futile.

At the SED station GIMEL (St. Georges VD), the refraction velocity images both from shear and compressional wave analysis show similar structures. The validity of velocity values in the bedrock is constricted in depth due to methodological inherent limitations. The MASW figures are in the same range as the values obtained from the shear wave diving wave refraction tomography surveys.

4.4 The Geophysical Interpretation

The most conclusive information about the subsurface structures is provided by the results of the hybrid seismic section (v_p-refraction tomography profiling and reflection seismic section) and confirmed by the evaluation results of the v_s-refraction tomography data.

As can be seen from the v_s and v_p refraction tomography sections in Fig. 3.2e/f & Fig. 3.4g/h, the topography of the bedrock surface is imaged in detail on both profiles. The geological interpretation of the seismic events is shown in Fig. 4.2a. The rock surface seems to outcrop to the South and almost to the North. Near to the SED station, a local depression in the hard rock topography is imaged with a depth of 7 m. Two apparent tectonic faults are indicated with black dashed lines.

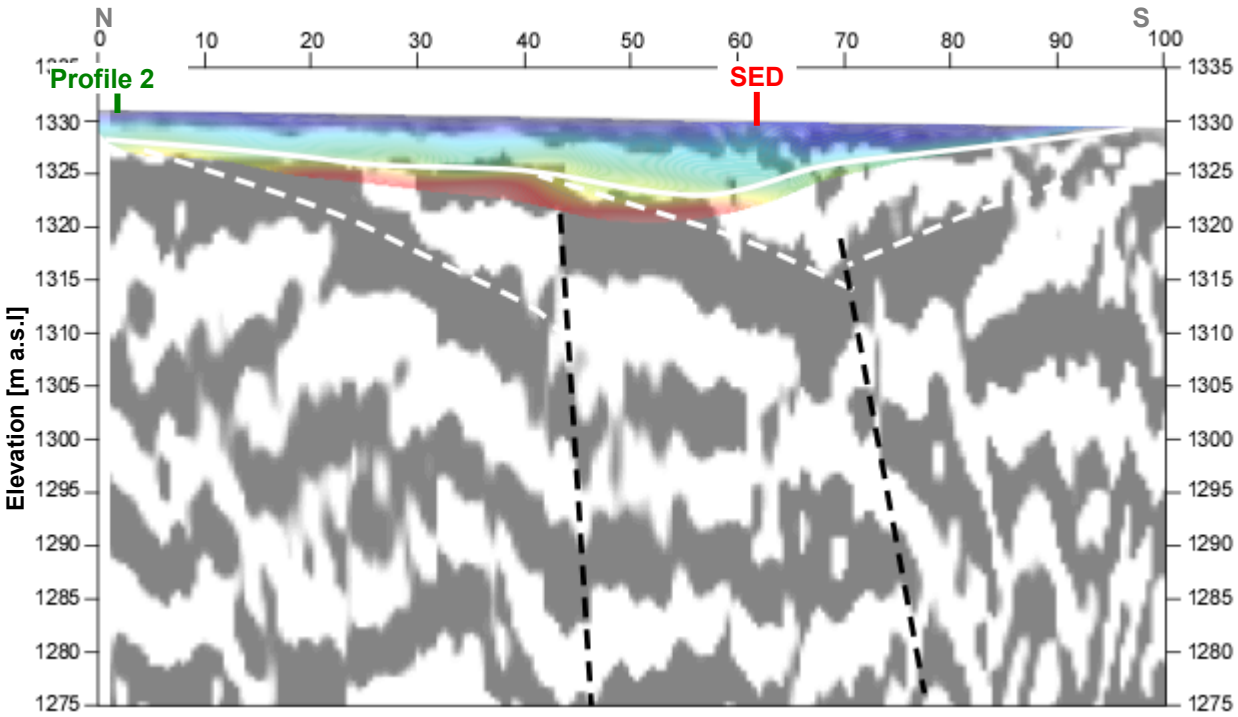

Fig. 4.2a Geophysical interpretation of the hybrid seismic section 09SN_08GIMEL-P1. White lines denote layer boundaries, continuous line the bedrock surface. The black dashed lines are indicative of suspected faulting.

The geological interpretation of the seismic events of line 09SN_08GIMEL-2 is shown in Fig. 4.2a. Also on the second hybrid section 09SN_08GIMEL-2, the topography of the bedrock surface is imaged in detail all over the profile. The maximal depth of bedrock topography seems to be in 5 m. Three areas in the bedrock with reduced velocities can be located and are interpreted as loosened rock, potentially by karstic processes. An apparent tectonic fault correspond with one of the loosened areas in the middle of the line.

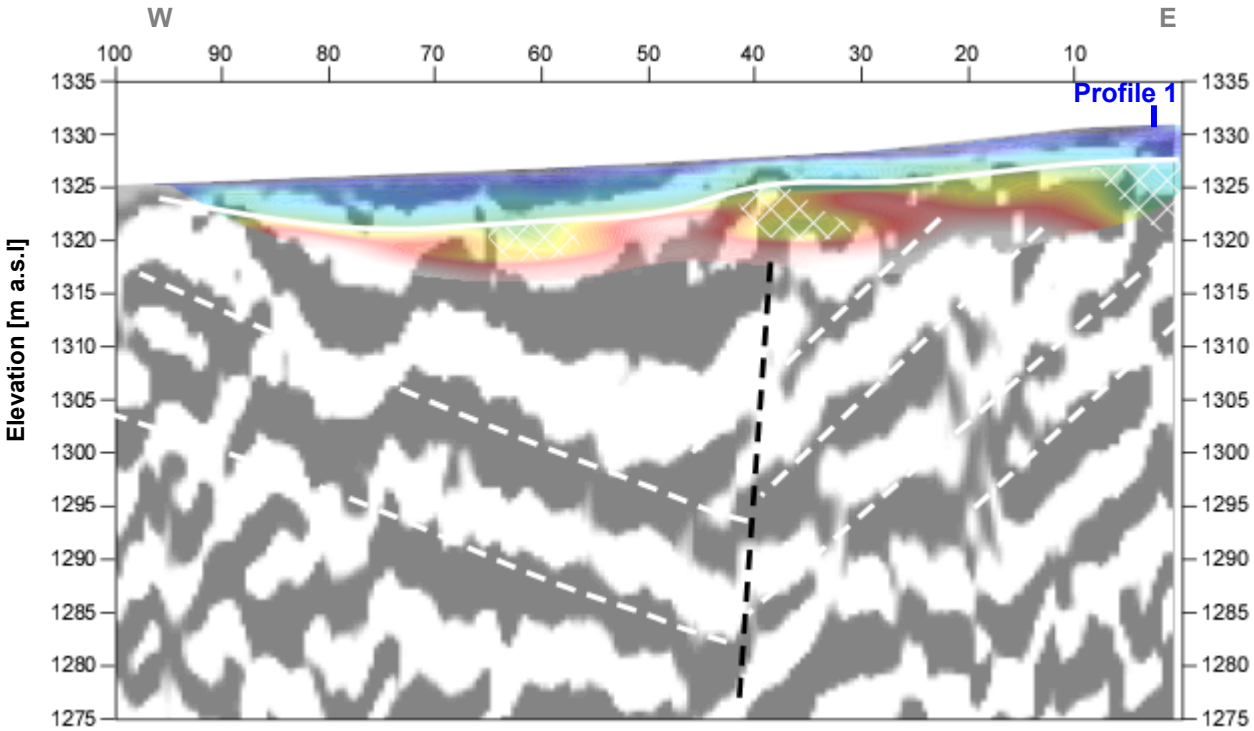

Fig. 4.2b Geophysical interpretation of the hybrid seismic section 09SN_08GIMEL-P2. White lines denote layer boundaries, the continuous one marks the bedrock surface; the black dashed line is indicative of suspected faulting. White hatched area correspond with a loosening zones (maybe karst).

5 SUMMARY AND CONCLUSIONS

- In May 2009 a combined seismic s- and p-wave survey was carried out at the SED earthquake monitoring station GIMEL near St. Georges (VD).
- The shear wave data have been evaluated by conventional diving wave refraction tomography techniques in order to derive the s-wave velocity field along the seismic line. The reached depth of investigation with reliable velocity values is in the range of 15 m.
- The p-wave data have been processed
  - firstly to derive a 2D s-wave velocity field by using the MASW (**M**ultichannel **A**nalysis of **S**urface **W**aves) technique;
  - and secondly, according to the hybrid seismic data processing scheme for representing the subsurface structures in a combined reflection seismic section with the superimposed p-wave velocity field.
- The shear wave velocity range determined by the MASW method in the uppermost 30 meters spans from values of 1073 to 2075 m/s.
- The scalar values derived by the MASW survey at the SED station are the following:

line 1			line 2		
$v_{s,5}$	=	1426 m/s	$v_{s,5}$	=	1512 m/s
$v_{s,10}$	=	1345 m/s	$v_{s,10}$	=	1473 m/s
$v_{s,20}$	=	1319 m/s	$v_{s,20}$	=	1408 m/s
$v_{s,30}$	=	1437 m/s	$v_{s,30}$	=	1503 m/s
$v_{s,40}$	=	1488 m/s	$v_{s,40}$	=	1550 m/s

- The maximum reliable refraction shear wave velocity is 2506 m/s at a depth of 15 m.
- The maximum p-wave velocity determined is 4984 m/s at a depth of 14 m.
- The geophysical interpretation of the subsurface structures in this report are to be validated and incorporated into a comprehensive appraisal by a geologist familiar with the local geological setting.

Schwerzenbach, 1st July 2009

Walter Frei
dipl. Natw. ETH
managing director

Lorenz Keller
dipl. Natw. ETH
project manager